Experimental assessment of mock calcifications in abdominal aortic aneurysm phantoms

---

Philippe Mahbeer

Biological and Biomedical Engineering
McGill University, Montréal

September 2021

A thesis submitted to McGill University in partial fulfillment of the requirements of the degree of Master of Engineering.

Table of content

List of Figures

List of Tables

Acknowledgements

I would like to thank my supervisor, Pr. Rosaire Mongrain, as well as my co-supervisor, Dr. Gilles Soulez, for their unconditional help in this project and for providing me with all the necessary resources to accomplish my research. Most of all, I would like to thank them for the guidance they provided, which was crucial for this project.

I would also like to express my gratitude to Stewart McLennan of McGill University for his great help in finite element models and analysis, and to Hongliang Li of the CRCHUM for his help in ultrasound imaging of PVA phantoms.

Finally, I would like to thank my greatest supporters in this endeavour: my family and friends. To my mother, Dominique; my father, Dennis; my brother, Thomas; and our newest family member, Arthur. They have always been there for me, always supporting me and pushing me to achieve my goals. Last but not least, my deepest thanks to the lovely Audrey Boily, who has been my rock in these difficult times. Thank you all for always being there when I needed you.

Abstract (English)

The development of phantoms, mock replicas of anatomical structures, has allowed cardiovascular research to improve stent grafts and various methods of insertion and deployment. Stent-graft deployment often occurs in aneurysms, large dilatations of the aorta, where calcification of the arterial wall may affect the treatment's efficiency. The experiment assessment of a mock calcified abdominal aortic aneurysm allows the evaluation of the impact of calcification on the arterial wall and the aneurysm. Using polyvinyl alcohol (PVA) hydrogel, the mechanical properties of the artery and the aneurysm can be replicated correctly; the addition of PVA/$CaCO_3$-based calcifications can then allow an examination of their impact on surrounding mock tissue through a series of tests on the phantoms: uniaxial tensile testing of mock arterial tissue with various degrees of calcification, finite element analysis of calcified tissue, and ultrasound imaging of calcified abdominal aortic aneurysm phantoms. At 15% strain, heavily calcified samples showed a significant load bearing effect, reducing wall stress up to 49% when compared to their non-calcified counterparts; this effect has, however, a small area of effect which can be clearly seen in smaller samples, while larger arterial phantoms could only demonstrate the effect locally in calcified areas.

Abstract (Français)

Le développement de fantômes, des modèles réplicant diverses structures anatomiques, ont permis aux chercheurs d'améliorer les méthodes de tests d'insertion de cathéters et les cathéters eux-mêmes. Or, le déploiement de cathéter se déroule principalement dans des anévrismes, de dangereuses dilatations de l'aorte, dont la calcification de la paroi artérielle peut affecter l'efficacité de ce traitement. L'évaluation expérimentale de fantômes d'anévrisme aortique abdominal calcifié permet de déterminer l'impact de la calcification sur la paroi de l'artère et de l'anévrisme. À l'aide d'hydrogel cryogénisé de polyvinyle d'alcool (PVA), les propriétés mécaniques de l'artère et son anévrisme peuvent être répliquées correctement; l'addition de calcifications faites à base d'un mélange de PVA et de carbonate de calcium ($CaCO_3$) peut ensuite permettre une évaluation complète de leur impact sur les propriétés de la paroi par une série de tests de tension d'échantillons de PVA calcifié à différents degrés, d'analyse d'éléments finis de tissus calcifiés et d'imagerie ultrasonore de fantômes d'anévrismes aortiques abdominaux calcifiés. À une déformation de 15%, les échantillons de PVA sévèrement calcifiés démontrent une réduction de contraintes dans la paroi de 49% comparé aux échantillons non-calcifiés; cette réduction est toutefois locale plutôt que globale, ce qui fait en sorte que cet effet n'est observé que dans les zones calcifiées de fantômes aortiques.

1. Introduction

Abdominal aortic aneurysms (AAA) are a life-threatening condition in which the abdominal aorta dilates to at least 1.5 times its normal size. Although both computer models and physical phantoms of AAA exist, these models rarely include other pathologies related to the AAA, such as the presence of calcification in the artery wall. These heterogeneously distributed deposits of calcium affect the mechanical properties of the vessel and result in a hardening of the vessel wall, which can lead to poor positioning of the stent graft or ineffective treatment. Most models that do take calcification into account are homogeneous models, where the entire vessel wall is calcified instead of having inclusions of calcium deposits. Therefore, this goal of this project will be to create an accurate patient-inspired phantom of a calcified AAA and determine the effects of calcification in the AAA phantom.

2. Background and literature review

2.1. Abdominal aortic aneurysm (AAA)

The aorta is the largest vessel in the human body. Being an artery, it transports the blood from the heart towards the rest of the body. The aorta originates from the left ventricle of the heart, where the newly oxygenated blood leaves the heart, and is characterized by five distinct areas: the ascending aorta, the arch of the aorta, the thoracic aorta, the abdominal aorta and the descending aorta [1]. The arch of the aorta is the peak of said artery, being in the shape of an inverted “U”, while the latter two segments of the aorta, the abdominal and descending aorta, descend along the posterior mediastinum down to the fourth lumbar vertebra (L4) where it bifurcates into the two common iliac arteries (Figure 2.1.1) [1].

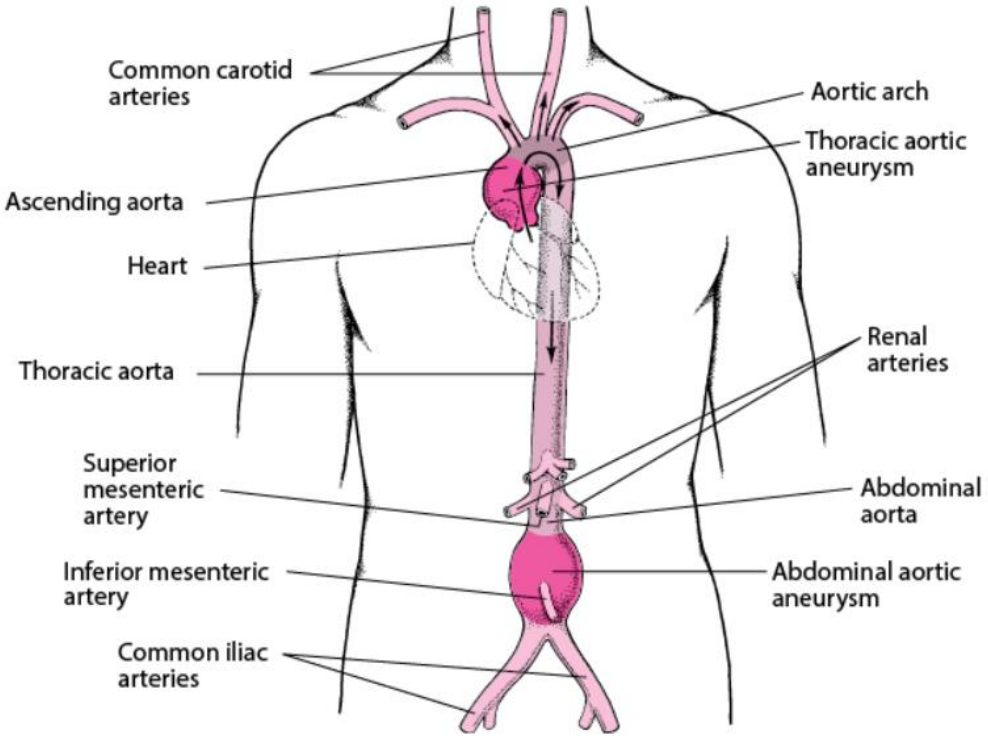

Figure 2.1.1. Anatomy of the aorta and the development of an abdominal aortic aneurysm in the abdominal section of the aorta. [41]

The aorta is composed of a heterogeneous mixture of various cells, such as smooth muscle cells, endothelial cells and fibroblasts, as well as extracellular matrix, elastin and collagen. Collagen I and collagen II account for up to 90% of the total collagen composition in this structure. Collagen concentration in the aorta has a significant role in the blood vessel's biomechanical properties, namely the dilatation and contraction of the aorta [2]. The arterial wall of the aorta is composed of three separate layers: the tunica intima, the tunica media and the tunica adventitia [3]. Each layer has a different chemical and biological composition, which leads to very different mechanical properties. The innermost layer, the tunica intima, is approximately 100 to 130 μm in thickness and is mainly composed of endothelial cells, which are responsible for secreting

chemicals causing arterial contraction and dilatation when oxygen is needed [4]. The middle layer, the tunica media, is thicker than the former layer, having a thickness of about 400 to 900 µm, and is composed of smooth muscle cells that control the pressure in the artery and the blood flow through a constant alternation of dilatation and contraction [5]. The third and outermost layer, the tunica adventitia, is approximately 200 µm to 300 µm in thickness and is structured into an arrangement of muscle cells and connective tissue to prevent the aorta's rupture during dilatation [5].

The abdominal aorta is a part of the aorta, the largest artery in the human body, which passes through the abdominal cavity. This section of the artery branches off into different organs and areas, most notably the renal arteries that bring blood to the kidneys, and the two large iliac arteries to the legs. The abdominal aorta bifurcates into the two iliac arteries near the fourth lumbar vertebra.

An abdominal aortic aneurysm is a dilatation of the infrarenal abdominal aorta [6]. This dilatation is caused by the progressive degeneration of the arterial wall, leading to an accumulation of blood in the arterial wall due to said weakness [7]. This dilatation is only considered an aneurysm when it expands more than one and a half times the regular diameter of the aorta; in this case, it would need to be over three centimetres in size from the summit of the aneurysm to the opposite arterial wall compared to the aorta's average diameter of two centimetres (Figure 2.1.2.a) [8]. Moreover, the degeneration of the wall and the stiffening is often linked to the development of an intraluminal thrombus (ILT), a large blood clot that forms within the vessel [9]. The ILT has different mechanical properties than the AAA and the vessel wall. In fact, an ILT is almost always present in larger AAAs, especially those of over 5.5 cm, which is the threshold at which AAA often have to be repaired through invasive or non-invasive maneuvers (Figure 2.1.2.b) [10]. The

presence of an ILT in the AAA is also very often associated with an early rupture of the AAA, which can lead to fatal bleeding if left untreated. However, some studies have shown that an ILT can reduce the wall stress depending on the shape of the AAA [8, 11].

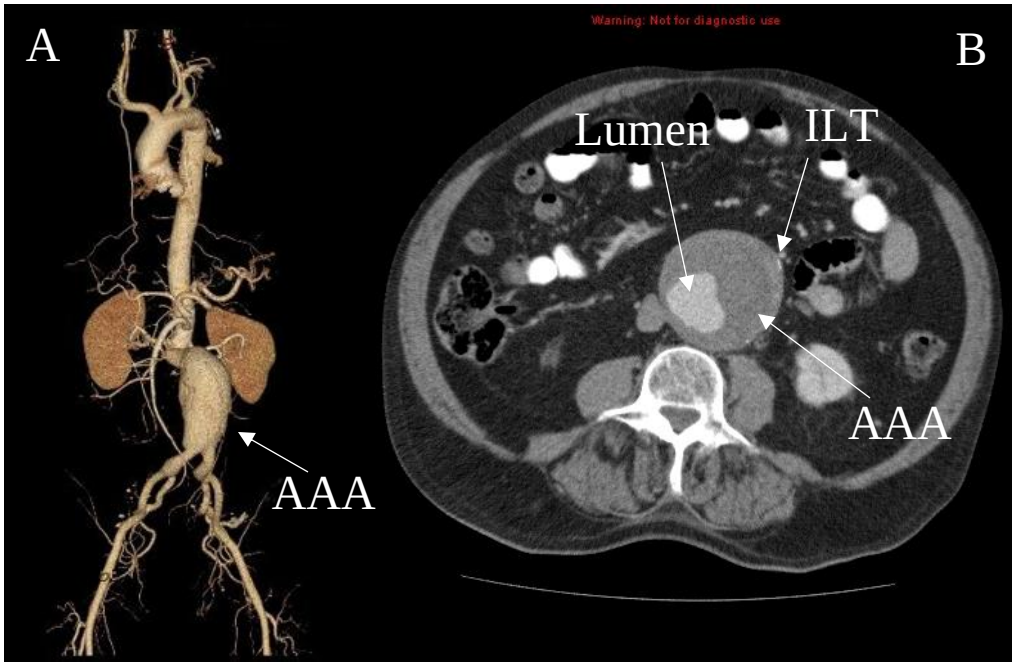

Figures 2.1.2. (A) Model reconstruction of an abdominal aortic aneurysm. (B) CT-scan of the aneurysm and its ILT. [42][43]

An AAA is dangerous for patients due to the fact that it may go unnoticed until it has grown considerably. It is often found by accident during medical imaging for another illness. One of the common signs of an AAA is the feeling of a second heartbeat in the abdominal cavity and sharp pain. Although rare in younger patients, it is much more commonly found in men over the age of 55 and women over 70 [12]. In fact, it is responsible for more than nine thousand deaths in the United States each year, the thirteenth leading cause of death [11 – 13]. The most common causes linked to the development of AAAs are similar to those linked to atherosclerosis and other cardiovascular diseases: smoking, a sedentary lifestyle, hypertension, lipid-rich food, genetics and

family history [14]. When patients start feeling pain, an ultrasound is usually done, where the AAA is often discovered. It is important to note that AAAs do not appear clearly on x-rays, though the calcium deposits that are present in the vessel wall do appear. The best method for detecting an AAA is by computed tomography scan (CT scan), since it is possible to identify both the AAA and the calcification (Figure 2.1.3) [15].

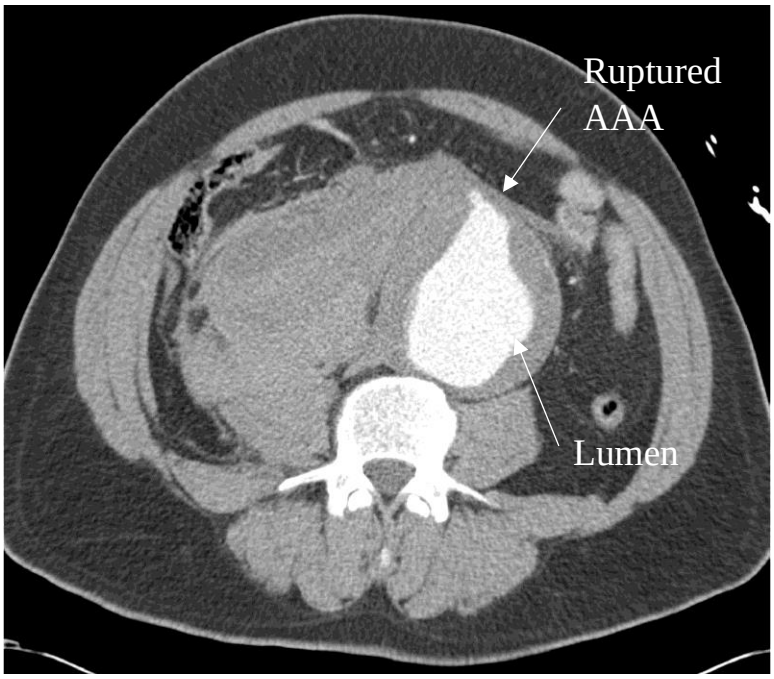

Figure 2.1.3. CT-scan of a ruptured AAA. [44]

2.2. Calcification

The calcification present in the arterial lumen and wall contributes to the hardening of the vessel wall and the changes in mechanical properties. The deposits can be either calcified, fibrous, fibrolipidic or lipidic [16]. Atherosclerosis and arteriosclerosis are among the different types of vessel degeneration that can occur, usually occurring in the lumen and the tunica media of the arterial wall. Calcium-based deposits occur more in the media and, being heterogeneously distributed calcified plaques, are often the result of the accumulation of calcium sediments in the

wall [3]. They are also believed to be the cause of stiffening of the AAA wall [3, 17]. They exhibit an almost linear stress-strain behaviour [18]. The degree of calcification of the aorta can vary greatly. The more calcium deposits there are, the stiffer the arterial wall. In the abdominal aorta, a mild level of calcification in the iliac arteries often develops before any other area [19]. As more calcium accumulates, the bifurcation of the aorta into the iliac arteries is the second place to exhibit calcium deposits, followed closely by the AAA wall lateral to ILT, then the AAA wall without ILT, and finally the proximal neck around the renal arteries. In her article, He et al characterized the different shapes of the calcium deposits into three specific groups: stones, strips and flakes (Figure 2.2.1) [20].

Figure 2.2.1. 3D reconstruction of the various shapes of calcifications found in patients: stone calcification (left), strip calcification (middle) and flake calcification (right). Calcifications not to scale.

Stones are roughly spherical or cubic calcium deposits, around a millimetre in diameter, while strips are deposits that are at least twice as long as they are wide and usually two to three times the length of stone-like calcifications. Finally, flakes have approximately the same width and length, but a thickness about a third of their length. Overall, stones and flakes are much more common, representing about 75% of all calcium deposits [20]. Furthermore, the shape of the

calcification is strongly associated with the volume of calcium in certain areas: for example, flakes are much more likely to be found at the bifurcation and the iliac arteries [19, 20].

The calcification of the arterial wall is thought to cause lesions and affect the wall stress, though whether it increases or decreases stress in nearby vessel wall has been the subject of a debate for many years. It is also unknown whether calcifications can contribute to tissue failure such as AAA rupture and how they affect endovascular repair (EVAR), a surgical method to repair AAA, which will be discussed in the next section [21]. In fact, it is believed that small stone-like and strip calcium deposits weaken the arterial wall due to their sharp edges, while larger and rounder flakes reduce stress due to their shielding effect [19]. An article by Maier in 2010 demonstrated through finite element simulations that calcifications in AAA exhibited significant load bearing effects and, overall, seemed to reduce the stress in adjacent vessel wall [22].

There are quite a few studies that have created physical models and phantoms in order to recreate AAA. A physical phantom of the AAA was made by He et al and included the ILT [23]. This phantom was made of polyvinyl alcohol cryogel (PVA-C), a hydrogel that underwent specific cycles of freezing and thawing to exhibit mechanical properties similar to those of the AAA and ILT. Regarding calcification and solid deposits in the artery, Pazos [24 – 25] created an interesting finite element model of the coronary arteries in the case of atherosclerosis, including the calcified segment in the artery, while Youssef [26] studied the creation of vascular calcification with PVA-C and calcium carbonate ($CaCO_3$).

2.3. Endovascular repair (EVAR)

EVAR is a minimally invasive surgery in which a stent graft (SG) is inserted in the aneurysm. This maneuver is done by inserting the SG through an incision on the leg, near the groin. The main advantage of said method is its minimal invasiveness: the alternative procedure,

abdominal surgery, is much more invasive and requires more time and tools to solve the same issue [27]. The SG is a graft surrounded by metallic supports, which are the stents. The main body of the SG is implanted in the AAA, while the legs are deployed in the iliac arteries (Figure 2.3.1) [28]. Simply put, this device, which is essentially a fabric tube supported by short metallic stents, reinforce the weaker areas of the aorta and stops the AAA from rupturing. The fabric can be made of various materials, such as Dacron or polytetrafluoroethylene [29].

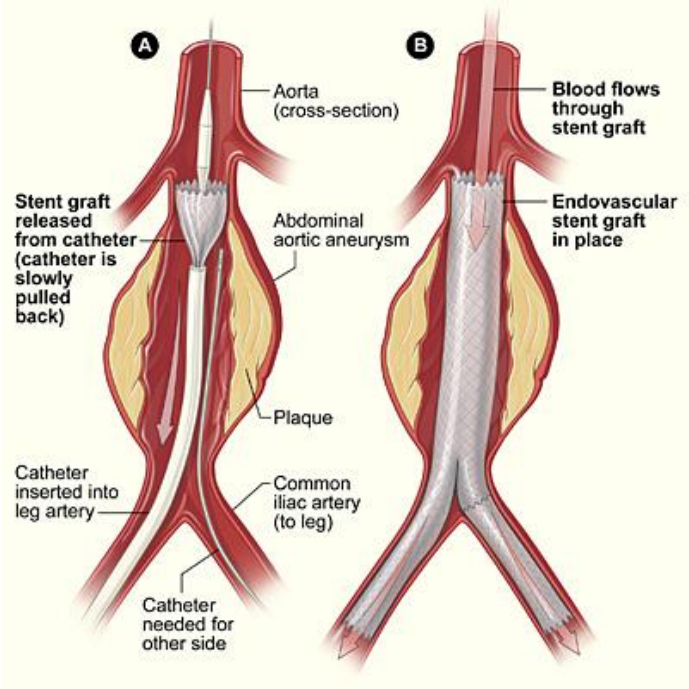

Figure 2.3.1. Steps of endovascular repair. [45]

The steps to perform EVAR are straightforward: the guidewire is first inserted in the femoral artery in the upper leg near the groin, then the catheter is inserted. Once the SG is correctly positioned in the AAA, it is deployed from the top of the AAA all the way down in one of the legs of the bifurcation of the iliac artery. This is followed by the insertion of another catheter in the

remaining leg of the bifurcation and the deployment of the last SG [29]. It is important to note that the SG deployed in the iliac arteries overlaps the SG in the AAA to create a strong and stable graft. This procedure is done using an x-ray machine to guide the placement of the SG in the artery.

As mentioned, the main advantage of performing an EVAR procedure rather than an abdominal surgery is that it significantly less invasive, which reduces the patient's recovery time [30]. Placing a SG in a patient also has multiple purposes. First, it isolates the aneurysmal sac from the blood pressure, therefore reducing the risk of rupture [27, 28, 30]. By also isolating the aneurysmal sac from direct contact with the blood flow, it stops blood from continuously accumulating in the aneurysm. Left untreated, the AAA may lead to fatal rupture and bleeding. Second, in some cases where the accumulation of calcium reduces the size of the lumen such as atherosclerosis, it re-establishes a regular blood flow through the aorta by expanding the lumen and compressing the plaques [30].

EVAR does present some issues. Although abdominal surgery is invasive, it offers better results than SG [27 – 30]. Primarily, the installation of a SG requires the deployment of its end sections in healthy tissue to avoid type 1 endoleaks. Type 1 endoleaks are the result of blood flowing back into the aneurysmal sack through the space between the ends of the SG and the arterial vessel wall [29]. SG navigation and fixation rely on medical imaging to deploy the SG in the affected calcified area, as well as its proximal and distal ends in healthy tissue. In order to avoid and prevent any complications or issues, regular follow-ups are required.

2.4. Polyvinyl alcohol (PVA)

Current research in the development of mock cardiovascular tissues is often done with polyvinyl alcohol (PVA) hydrogel. PVA hydrogel is the material of choice in many publications for its tissue-mimicking properties [23, 24, 26, 31]. PVA is able to sustain large deformation and

to be moulded into any shape with sub-millimetre thickness. It consists of a secondary alcohol group attached to a linear carbon chain, with said chain repeating itself. Therefore, its idealized chemical formula is as follows:

$$[CH_2CH(OH)]_n$$

where *n* represents the number of times this chain repeats itself [31]. This polymer forms a hydrogel, a viscoelastic substance capable of holding a substantial amount of water in its three-dimensional polymeric network. Hydrogel can retain a large quantity of water because of its hydrophilic functional group [32]. In fact, PVA used for its tissue-mimicking properties is made with a 9:1 water to polymer ratio.

PVA has been used to recreate cardiovascular structures for over a decade. Pazos et al developed a PVA phantom to mimic the mechanical properties of coronary arteries in 2009 [33]. He et al later developed a PVA phantom for AAA, which was then used to test the ability of PVA to mimic the mechanical properties of both the artery and its aneurysm grafted together [23]. In order to mimic the mechanical properties of the arterial wall, PVA must go through a certain number of cycles of freezing and thawing at specific temperature and controlled rates. PVA that undergoes this type of thermal cycling is then referred to as PVA cryogel, or PVA-C. The thermal cycling of PVA stimulates physical crosslinking in the PVA, which has the advantage of leaving no residual crosslinking agents in the cryogel [23, 31 – 33]. The number of cycles the hydrogel goes through changes its mechanical properties; this can be tuned to resemble the arterial wall's mechanical properties [34]. A number of parameters can be altered to induce changes in the underlying structure of PVA-C and its properties; said parameters being the number of freezing-thawing cycles, the freezing rate, the thawing rate, the maximum freeze holding temperature and the maximum thaw holding temperature [35]. Many studies have shown that crystallization and

phase separation, two important factors that contribute to the cryogel's internal structure, occur during the thawing rate: the former occurring in the first three freezing-thawing cycles and the latter in subsequent cycles [31 – 36]. Work done by Pazos illustrated the effects of increasing the number of thermal cycles the PVA undergoes [33]. A higher number of cycles leads to an increase in the gel stress response to stretching, while also reducing the matrix pore size. In other words, the more thermal cycles the PVA undergoes, the stiffer it becomes. Experimental data has shown that after 11 thermal cycles, the observed difference becomes non-significant [23, 33, 35].

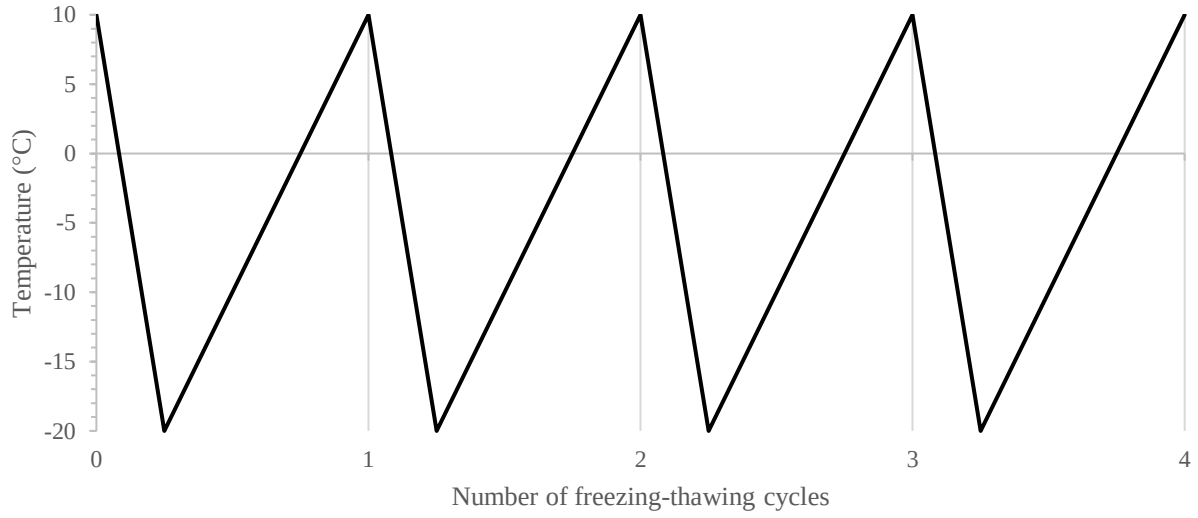

Figure 2.4.1. Thermal cycling of a PVA sample as the sample's temperature varies from 10°C to -20°C.

Further work done by He et al on the same subject demonstrated that the optimal number of cycles to mimic the arterial wall was between 6 and 8 [23]. Furthermore, the freezing and thawing rates have been proven to affect the mechanical properties of PVA-C, with the latter being the most influential. The thawing rate affects the formation of PVA-C, while the freezing rate affects the formation of ice crystals [33 – 35]. A thawing rate of 10°C/min is the highest that still

produces a cryogel, but a rate lower than 1°C/min is recommended for a finer control of the mechanical properties [35].

3. Experimental protocol for PVA phantoms and mock calcifications

3.1. Extracting the calcifications

Calcifications models used in mock arteries needed to be extracted from patient's CT-scan images in order to have patient-based models. Through the use of the *ITK-SNAP* software, CT-scan image stacks were analyzed, and calcifications were identified [39]. When contrasted to tissue, calcifications appeared as bright white spots a few pixels in size. Manual segmentation of these bright spots in each image of the CT-scan image stacks allowed the user to clearly identify the relevant voxels and isolate the calcifications from the surrounding tissue. Although automatic segmentation may have worked in identifying large calcifications, setting a working threshold to identify all calcifications, especially the smaller stone-like and strip-like calcifications, in an image was not optimal, since most smaller calcifications were not detected by the algorithm.

Once calcifications were segmented, the segmented image stack weas imported into 3D modeling software for analysis. In this case, *Meshmixer* (Autodesk, Inc.) was used to mesh the segmented image stack into calcification models, as seen in Figure 3.1.1 below. The triangular mesh size was adjusted to the order of 10^{-4} to 10^{-5} m. Doing so allowed the creation of accurate, patient-based structures.

These three-dimensional structures were then classified into one of three categories: stones, strips and flakes. In each group, the calcification that embodied the most the ideal model of its group based on its shape and size was selected and used to make a mold.

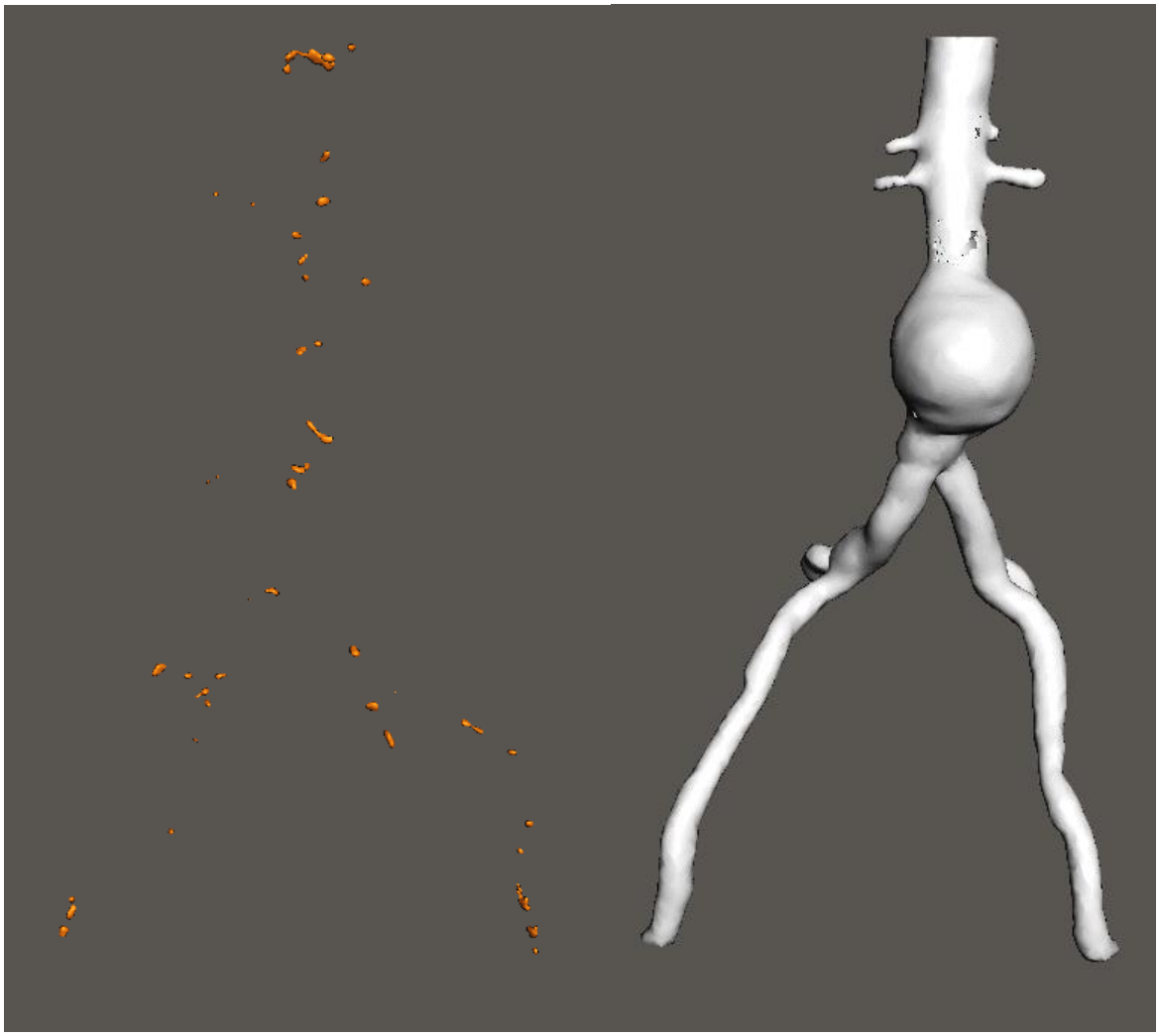

Figure 3.1.1. Left: 3D mesh of the calcifications in the aorta and the iliac arteries. Right: Mesh of the abdominal aorta, the iliac arteries, the renal arteries, and the aneurysm.

3.2. PVA recipe

PVA was used to replicate the mechanical properties of the aorta. In order to use it in moulds, it first had to be prepared in laboratory. The initial step was to mix a 9:1 water to PVA ratio by weight in a beaker under a chemical hood; in other words, 9 grams of water was be added to the mix for every gram of PVA powder present in the beaker. Since PVA is a hydrogel, water was its main component. Once the water and PVA powder were thoroughly mixed with a small

spatula, the new mix was poured into an Erlenmeyer flask in which a magnetic stir bar was added; the Erlenmeyer was then placed on a magnetic hot plate stirrer at a temperature of 100°C. The PVA mix remained on the plate until it reached an internal temperature of 100°C: at that temperature, the PVA mix changes colour from a milky white to mostly transparent, while the air bubbles that were initially in the mix start dissipating. Once the mix was clear and free of air bubbles, the PVA could then be poured into the mould and sealed. Ideally, the mould would then have been placed on a temperature-controlled Peltier plate, with specific freezing and thawing temperatures and rates; however, Peltier devices cannot support all sizes of mould. In the case of an AAA, a standard Peltier device was too small to adequately treat the PVA in the mould of the artery: the mould was instead placed in a freezer and subsequently in a refrigerator to induce the freezing and thawing cycles. Although the freezing and thawing rates were not exactly the same as the Peltier's automated rates, it was possible to set the freezing and thawing temperatures to -20°C and 10°C, respectively, and still obtain PVA with similar properties to that of Peltier-made PVA when compared to values of previous studies. To mimic the mechanical properties of the arterial wall and the AAA, the mould was subjected to 8 freezing-thawing cycles of 9 hours, with half that time, 4 hours and 30 minutes, spent in the refrigerator and the other half in the freezer.

3.3. PVA and calcium carbonate mix (PVA/$CaCO_3$)

Calcifications that were meant to be inserted in the PVA samples were made in a similar fashion to the baseline PVA mix. However, there was an additional ingredient to the 9:1 W/W water-to-PVA mix: calcium carbonate ($CaCO_3$). Before adding the PVA powder to water, CaCO3 was added to the PVA powder at a ratio of 1.45:1 W/W CaCO3/PVA, based on the research of Youssef which showed that this mix gave the strongest mix of calcium carbonate and PVA [26]. Although its composition differs from that of real calcifications found in the AAA, it still had

mechanical properties that resembled those of real-life calcifications, which will be discussed in the next section. Once the calcium carbonate and PVA powders were mixed, they were added to the volume of water, till the 9:1 W/W water/PVA ratio, then heated and mixed for approximately an hour and finally subjected to 8 freezing-thawing cycles (Figure 3.3.1). The addition of food colouring liquid in the mix after the heating process gave the calcifications a distinct tint that allowed them to be easily identified when inserted in a phantom without changing its mechanical properties (Figure 3.4.1). The resulting sample was a uniform PVA and calcium carbonate sample.

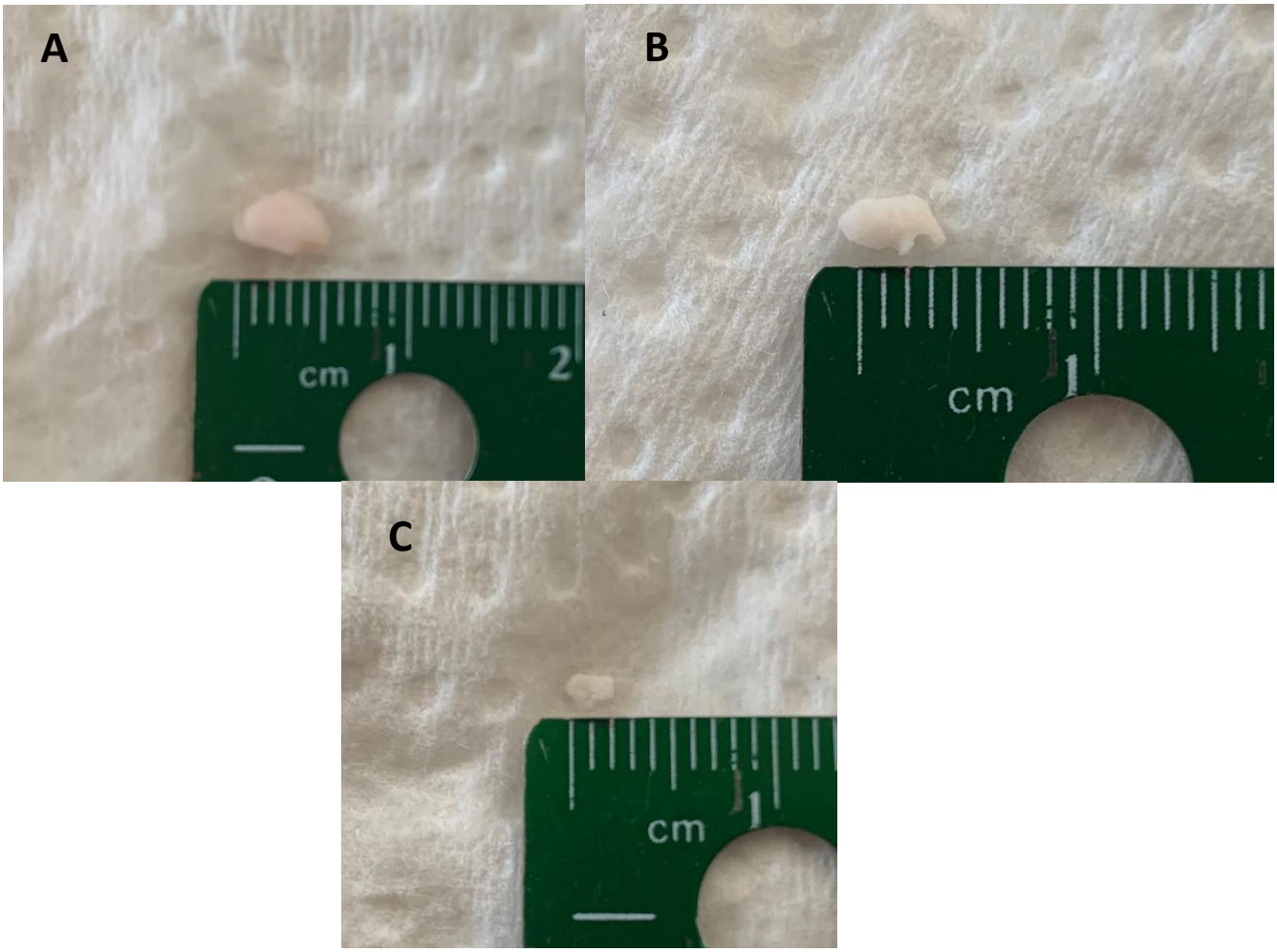

Figure 3.3.1. PVA/CaCO3 calcifications and their respective sizes. (A) Flake calcification; (B) Strip calcification; (C) Stone calcification.

3.4. Uniaxial tensile testing samples

In order to assess some of the mechanical properties of mock calcified abdominal aortic aneurysm and its surrounding mock tissues, uniaxial tensile tests of PVA samples with calcium carbonate calcifications needed to be done. These samples had to satisfy a few factors: they needed to have a thickness of 2 mm to 2.5 mm, a surface area of over 2 cm^2, and be mass-produced in a short amount of time. Moreover, the uniaxial tensile tests were done to test three factors: the effect of the calcifications' depths in the arterial wall, the effect of the calcifications' shape and size, and the effect of the area covered with calcifications. Small square samples of approximately 15 mm by 15 mm by 2.5 mm were produced by 3D printing a 4x4 square grid moulds of the samples, for a total of 16 moulds in which to pour the PVA.

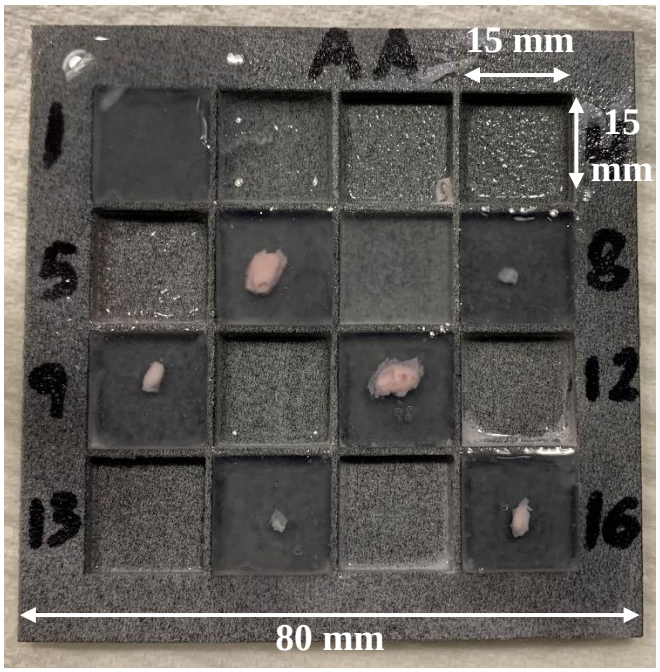

Figure 3.4.1. Plate for uniaxial tensile testing samples.

First of all, to test the effect of the calcifications' depth in the arterial wall, a single calcification was introduced in the sample before the start of the freezing-thawing process (Figure 3.4.1). To make a sample in which the calcification is in the middle of the sample on all axes, the mould was half-filled with PVA, after which the calcification was added to the centre of the mould, then the mould was filled to the brim with additional PVA before being subjected to 8 freezing-thawing cycles. In the case of samples with a calcification closer to the surface, the mould was filled to three-quarters of its maximum capacity and a calcification was placed directly in the center of the sample, then the remaining PVA was poured over to fill the mould. Of note is the presence of a single calcification instead of many: the freezing-thawing process causes an expansion and contraction of the gel-like PVA into a more solid form, which may displace the calcifications present within the gel. It was much easier to control and assess the depth of a single calcification than a large number of them, which could give much clearer results, and reduce biases and uncertainties.

Second, to test the effect of calcifications' shape and sizes, samples were prepared in a similar fashion to previous samples, with the exception that all samples were made with multiple calcifications placed in the samples after the mould was half filled in order to have them in the middle of the sample. Samples were separated into three groups based on the shape of the calcifications present within the PVA: the flakes, the large and irregular calcifications; the stones, the round pebble-like calcifications; and the strips, the long cylindrical calcifications. For each group of calcifications, two different types of samples were made: mild calcifications, meaning calcifications would only span approximately 1 cm^2 on the sample, and heavy calcifications, where the calcifications would span over 2 cm^2 in surface area.

Finally, samples were made to replicate the clinical conditions in which we find the calcium deposits. Based on a study by He et al, calcifications within the arterial wall are usually found in combinations of various shapes and sizes: stones and flakes, strips and stones, or stones, strips and flakes altogether [20]. Similarly to the previous samples, each of these three groups were tested with both mild and heavy levels of calcifications.

Testing of these calcified samples was done with a uniaxial tensile testing machine (Enduratec ELF 3200, Bose). To ensure consistent results, all samples were held with small hooks at each corner at a distance of approximately 2.5 mm from each side (Figure 3.4.2). The hooks were then held tightly in the clamps of the uniaxial tensile testing machine and the sample in place was pre-loaded at 0.05 N to keep it under tension. Hooks were used instead of clamps to hold the samples due to the very slippery and viscoelastic nature of PVA, making hooks a sure-fire method of holding the sample in tension without risk of slipping.

Once the sample in place was pre-loaded, it was subjected to preconditioning: the sample was stretched 6 times at a rate of 0.06 mm/s to a maximal displacement of 6 mm. Finally, the acquisition of experimental data could begin. The sample was once again pre-loaded at 0.05 N, then pulled upwards at a rate of 0.1 mm/s until a maximal displacement of 6 mm. Although the goal was to study stress accumulation at 15 % strain, which represents the approximate strain rate of the abdominal artery, the sample was stretched up to 30 %. All samples were tested in triplicate, with only some samples tested in duplicate due to rupture during the installation or preconditioning.

Figure 3.4.2. Uniaxial tensile testing of PVA samples on mechanical tester. Samples were hooked at each corner.

Following uniaxial tensile testing, uniaxial compressive testing was done on 10% of all previous samples to examine adherence between the PVA sample and its embedded calcifications. As the samples are the result of a heterogeneous mix between PVA and calcifications, adherence may be an issue, since low adherence between the PVA and the calcifications could lead to pockets dissipating the stress. Selected samples were initially clamped at each end, then compressed at a rate of 0.1 mm/s for 100 seconds, leading to a compressed PVA sample. Afterwards, samples were

transversally bisected, and adherence was observed between the PVA and the calcifications by trying to manually separate the layers of PVA and PVA/$CaCO_3$.

Sample composition	n
PVA	3
PVA/CaCO3	2
Single flake - Middle	3
Single stone - Middle	3
Single strip - Middle	3
Single flake - Surface	3
Single stone - Surface	2
Single strip - Surface	3
Flakes - Mild	3
Stones - Mild	3
Strips - Mild	3
Flakes - Heavy	3
Stones - Heavy	3
Strips - Heavy	3
Stones & Strips - Mild	3
Stones & Flakes - Mild	3
Stones, Strips & Flakes - Mild	3
Stones & Strips - Heavy	3
Stones & Flakes - Heavy	2
Stones, Strips & Flakes - Heavy	2

Table 1. Uniaxial tensile testing samples with their respective calcification shapes, orientation and calcium deposits levels.

3.5. Finite element models

Finite element models of single calcification uniaxial tensile testing samples were created to study stress concentration around the calcification and its possible load bearing effect. A model of the uniaxial tensile testing was initially created in *Solidworks* (Dassault Systems) with the same dimensions as the samples: small square samples of 15 mm by 15 mm by 2.5 mm. Models were made with a single calcification within. Four models were made: a plain slab of arterial tissue, a flake calcification sample, a stone calcification sample, and a strip calcification sample. Each calcification was centered in the arterial tissue model and defined with an adherent contact between both surfaces.

These samples were defined with the material properties of the human artery rather than that of PVA, mainly due to the fact that the material properties of the human artery have been previously used in other works and theoretically create the same mechanical response to that of PVA in a similar situation [37, 38]. The various layers of the artery were not taken into account. A Yeoh hyperelastic material was used to define the modelled samples. Material constants of 0.174 MPa and 1.881 MPa as C_{10} and C_{20}, respectively, were used in a second order Yeoh hyperleastic material strain energy function, defined as:

$$W = C_{10}(\overline{I_1} - 3) + C_{20}(\overline{I_1} - 3)^2$$

Calcifications, on the other hand, being much stiffer than the arterial wall, were defined as an isotropic elastic material. Calcifications have variable mechanical properties, so the model calcifications were defined with an elastic modulus of 50 MPa and a Poisson's ratio of 0.4 [37]. Each model had a mesh size of approximately 23 000 – 25 000 nodes and 14 000 – 15 000 elements. The finite element solver used was Mechanical (*Ansys*).

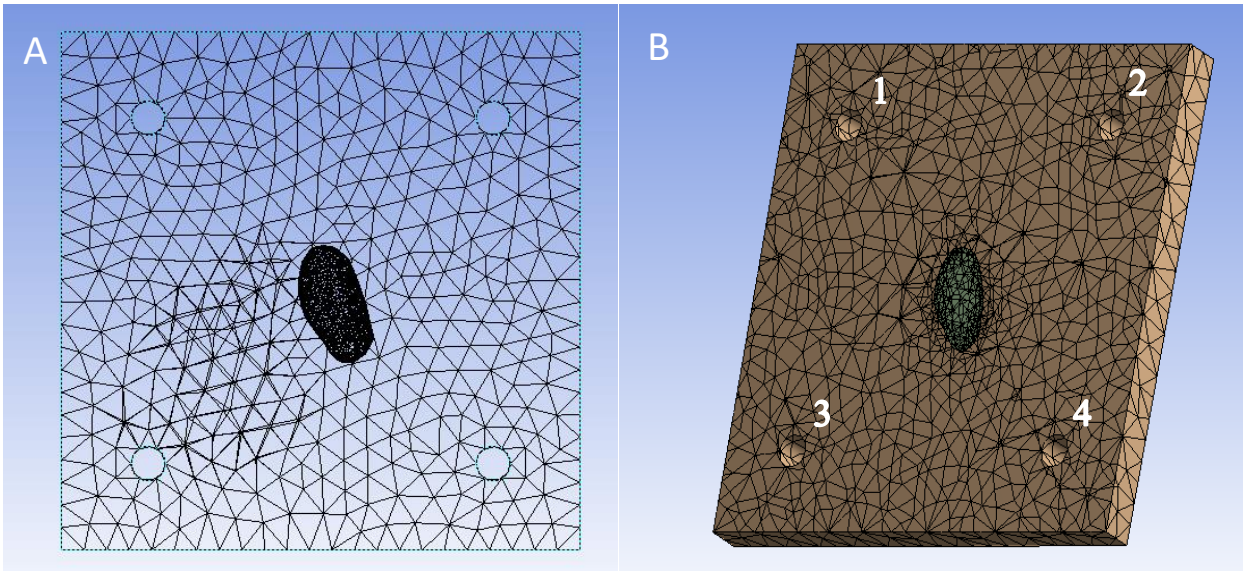

Figures 3.5.1. (A) Mesh view of the strip calcification model, with a single strip calc in the middle of the sample. (B) Cross-section view of the model. Holes numbered in a clockwise fashion.

The uniaxial tensile tests required fixing the two lower holes, while inducing a 15% strain in the model starting from the two upper holes (Figure 3.5.1.b). At 15% strain, the models were analyzed and the equivalent Von Mises stress surrounding the calcifications could be determined.

3.6. AAA phantom

PVA phantoms made to mimic arteries have been studied and developed for over a decade. These phantoms are usually made by 3D printing a mould of the phantom split into many parts: the inner mould to create the lumen of the abdominal aorta with a diameter of 22 mm, an exterior mould to surround the inner mould and form a circular phantom of approximately 2.5 mm in thickness in which the PVA can be poured, and caps at each ends of the phantom to seal the PVA during the freezing and thawing process. In this case, to test the implementation of the calcifications in the phantom, a simple tube-like phantom was designed with a large aneurysm of 1.5 cm on the upper half of the phantom.

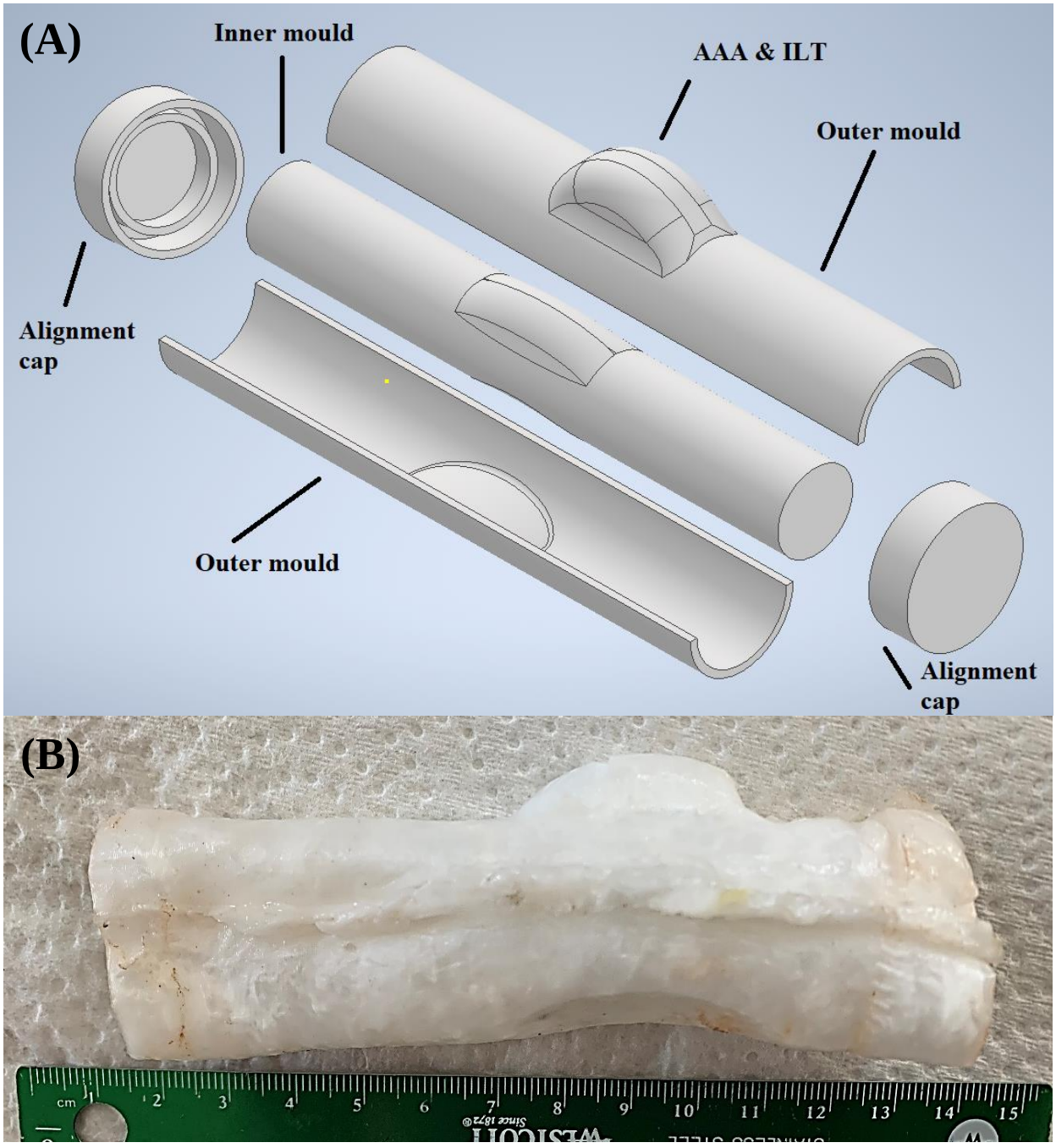

Figure 3.6.1. (A) Exploded view of the moulds to make the AAA and the ILT. (B) PVA phantom with AAA grafted at the top.

The AAA fused to the top of the phantom, a semi-circular protrusion rising over 1.5 cm above the external wall of the phantom and measuring over 4 cm in length, was filled with PVA to mimic its mechanical properties.

Although the AAA and ILT were also made of PVA, they were much softer than the PVA used for the arterial wall. To do so, the PVA underwent only 5 freezing and thawing cycles, rather than the 8 cycles the rest of the phantom underwent [23]. The development of the abdominal aortic aneurysm phantom occurred in two steps: the first being the setup of the arterial wall, the second being the insertion of the AAA and the calcifications. Calcifications could only be introduced in the phantom at the time the AAA and ILT were placed, since the AAA also needed to be fused to the wall of the mock artery. Therefore, before filling the mould, a piece of plastic was inserted in the AAA to completely block the entry of PVA within during the first 3 freezing and thawing cycles.

The phantom was then filled with PVA, sealed at each end with the caps, and subjected to 3 freezing and thawing cycles. Following this step, the outer shell of the mould was opened, the plastic sealing the AAA was removed as well as parts of the lateral wall of the phantom near the AAA, and calcifications are placed along the removed arterial wall and the AAA, followed by the addition of PVA to fil the empty space. The mould was then sealed again and subjected to an additional 5 freezing and thawing cycles, after which the outer shell was removed. The inner mould forming the lumen was carefully removed from the phantom by slowly twisting the mould in a clockwise manner as to not rupture the phantom when removing it. To measure the mean strain within the phantom and in areas filled with calcifications, while reproducing *in vivo* conditions, the AAA phantom was inserted in a closed-loop setup connected to a pump (Dual Phase Control Pump, Harvard Apparatus). This tube assembly, as seen below, was filled with water to simulate blood flow and pressure in the artery. By submerging the phantom in a tank full of water and connecting each end of the phantom to the open ends of the tubes, the phantom created a closed loop in which water could flow from the pump to the phantom and back to the pump through the

tube assembly. Water flow was pumped to an output phase ratio of 35/65 to imitate the systole to diastole time ratio at 20 cm^3 per stroke.

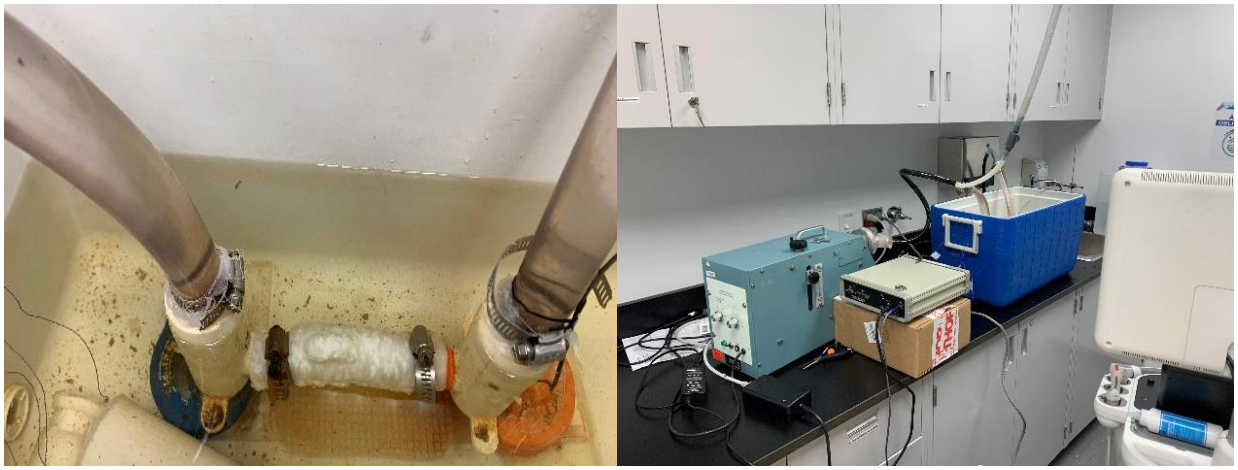

Figures 3.6.2 and 3.6.3. Left: Underwater PVA phantom fixed to two tubes allowing continuous pulsatile flow within the model. Right: Laboratory setup for PVA AAA phantom testing; the phantom is installed in a large water container, the pump ensures continuous flow, and the ultrasound machine allows transverse imaging of the phantom.

Once in place, the assembly was left to rest for 5 minutes to ensure proper installation: any errors in installation, whether it be poor tightening of the phantom, a rupture of said phantom or a loose connection between tubes, inevitably led to leaks in the tube assembly and water flowing back into the tank. When no leaks were detected, the pump was activated, and a linear ultrasound transducer was placed directly above the apex of the aneurysm. Expansion and contraction of the arterial wall could then be observed, and the strain analyzed afterwards. As seen in Figure 3.6.4 below, speckle could be observed in the lower half of the ultrasound image of the arterial phantom, which demonstrates the echogenicity of the phantom and its compatibility with ultrasound imaging.

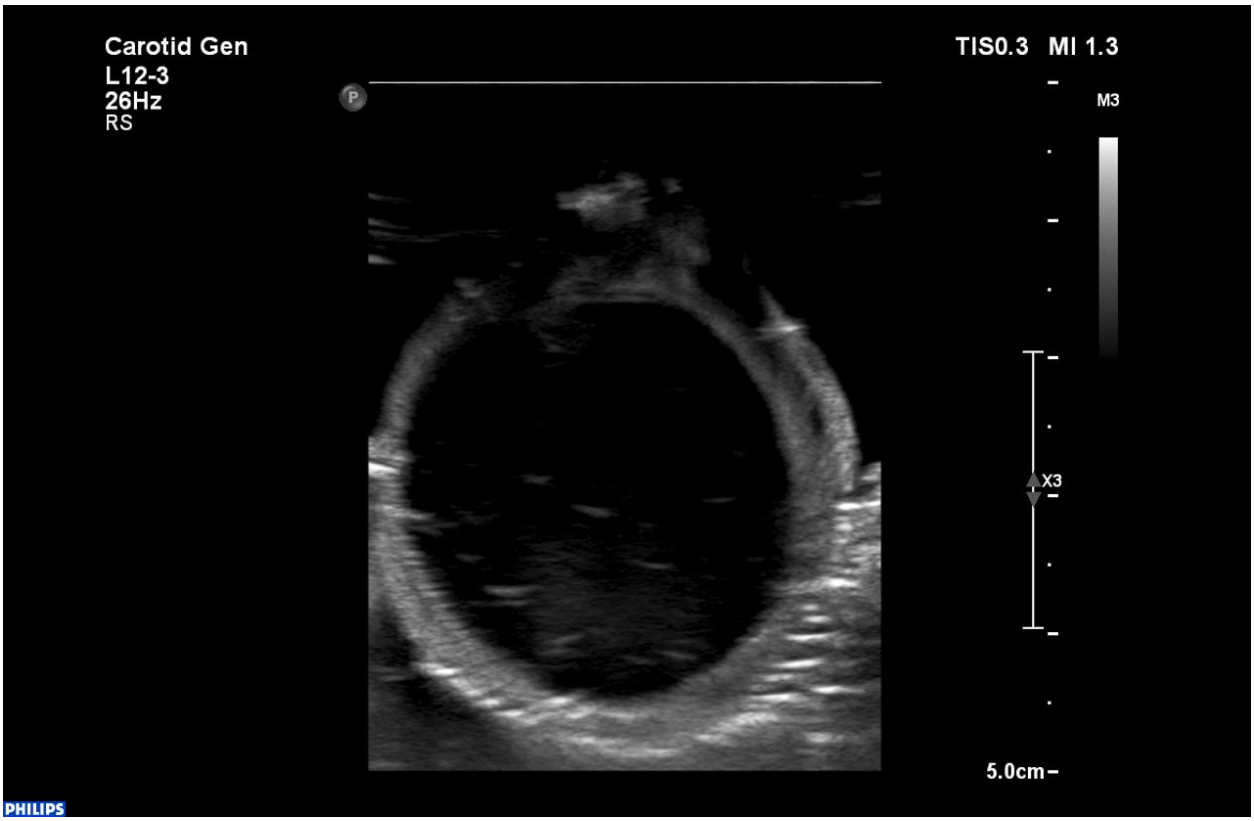

Figure 3.6.4. Transverse ultrasound image of the phantom. The lumen, the inner and outer wall of the arterial wall is clearly seen, the ILT (top) is difficult to see due to probe proximity.

4. Results of the mechanical characterization of PVA samples

4.1. Uniaxial tensile tests

Uniaxial tensile testing of square PVA samples filled with calcium deposits turned out to have very interesting results. Three different parameters were tested in the samples: the calcifications' depths in the arterial wall, the calcifications' shape and size, and the surface area covered with calcifications.

The first step before testing calcified samples was to determine the global uniaxial tensile stress of the PVA mix itself after 8 freezing and thawing cycles. As this PVA mix was the basis of every other sample, it was important to determine whether the PVA mix had the right composition and mechanical properties after the freezing and thawing cycles; were that not the case, this ill-prepared PVA mix would have an important effect in the subsequent samples. In this case, the PVA that underwent 8 freezing and thawing cycles was determined to have a similar stress response at 15% strain to the PVA found in other studies [23, 33]. As mentioned before, all samples were tested in triplicate (N = 3) with the Enduratech ELF 3200; only four types of samples had to be tested in duplicate (N = 2) due to sample rupture during the installation. Following the PVA uniaxial tensile test, another test was done on the PVA/$CaCO_3$ mix used to make the calcifications. The 145% W/W CaCO3/PVA mix proved to have a much higher stress response at 15% strain than the plain PVA samples, with an increase of over 50% in stress (Table 2) [26]. Afterwards, all samples were tested, and a general trend was observed rather quickly. In fact, as seen in Table 2, as the surface area covered in calcifications increased, the general wall stress seemed to decrease to the point where some samples showed a decrease of up to 40% compared to the non-calcified PVA samples, henceforth known as baseline PVA.

Sample composition	Wall stress at 15% strain (kPa) (Mean ± Standard Deviation)	n	% variation
PVA	15.28 ± 2.60	3	-
PVA/CaCO3	24.17 ± 1.25	2	58.17
Single flake - Middle	13.06 ± 5.23	3	-14.55
Single stone - Middle	15.42 ± 0.68	3	0.91
Single strip - Middle	17.50 ± 4.01	3	14.54
Single flake - Surface	15.00 ± 4.26	3	-1.82
Single stone - Surface	13.33 ± 2.08	2	-12.73
Single strip - Surface	13.75 ± 4.25	3	-10.00
Flakes - Mild	13.61 ± 0.98	3	-10.91
Stones - Mild	13.19 ± 0.71	3	-13.64
Strips - Mild	12.36 ± 1.04	3	-19.09
Flakes - Heavy	13.61 ± 3.09	3	-10.92
Stones - Heavy	11.67 ± 2.12	3	-23.64
Strips - Heavy	10.84 ± 1.23	3	-29.08
Stones & Strips - Mild	9.86 ± 2.39	3	-35.46
Stones & Flakes - Mild	9.72 ± 0.20	3	-36.37
Stones, Strips & Flakes - Mild	7.78 ± 0.20	3	-49.08
Stones & Strips - Heavy	8.06 ± 0.71	3	-47.28
Stones & Flakes - Heavy	7.92 ± 1.25	2	-48.18
Stones, Strips & Flakes - Heavy	9.17 ± 0.42	2	-40.01

Table 2. Wall stress of PVA samples at 15% strain. Samples were separated into four categories: the model samples for PVA and calcium carbonate; the calcification depth group; the single calcification shape group; and the clinical group.

Means and standard deviation were used to compare results between samples. Unsurprisingly, the calcium carbonate mix, with a wall stress over 50% higher than baseline PVA, could be considered different. However, most samples showed a strong overlap in standard

deviation with the baseline PVA; in fact, only samples mimicking clinical conditions in mild and heavy calcifications had no overlap with baseline PVA.

4.1.1. Surface vs middle – The effect of single calcification's depth on surrounding tissue

A closer look at the samples in each category in Figure 4.1.1 painted an interesting picture regarding the relationship between calcifications and their effects in PVA samples. When observing the effect of a single calcification's depth on the surrounding area, it seems that depth has a stronger effect on stress concentration in samples with small calcifications such as stones and strips.

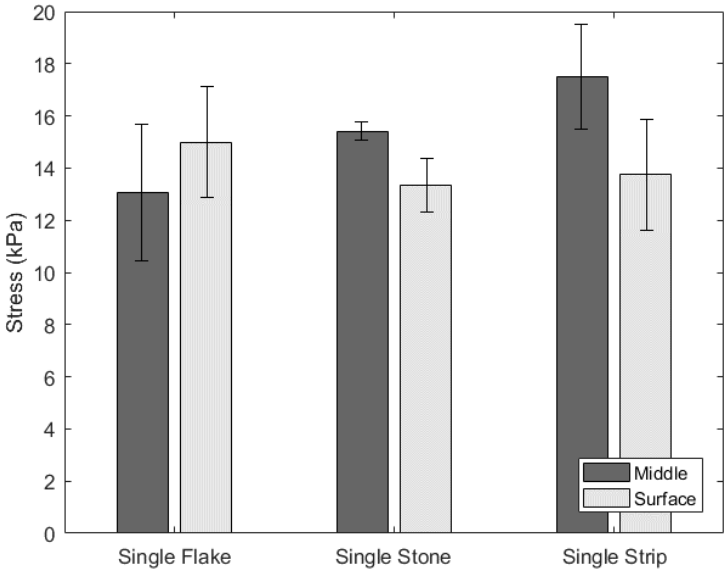

Figure 4.1.1. Comparison of the wall stress of calcified samples based on the calcifications' depths in the PVA sample. A lone calcification of different shape was either placed in the middle of the sample (dark grey) or close to the surface (light grey). N= 3, except the Single Stone – Surface samples (N=2).

Standard deviation bars overlapped strongly in flake calcification samples, while barely overlapping in stone and strip calcification samples. In fact, stone calcification embedded in the

middle of the samples showed very little variation compared to the baseline PVA (15.28 ± 2.60 kPa); this low variation is also shared with surface flake calcification samples. However, every sample's wall stress was close to 15 kPa at 15% strain, especially when taking their respective standard deviation bars into account.

4.1.2. Mild vs heavy calcification level – The effect of calcifications' shape on the surrounding tissue

Although the wall stress of mildly calcified samples, most notably the flake samples, remained somewhat close to the wall stress of the baseline PVA in Figure 4.1.2, an overall decrease was observed as the calcification level is increased from mild to heavy, with the exception of flake samples.

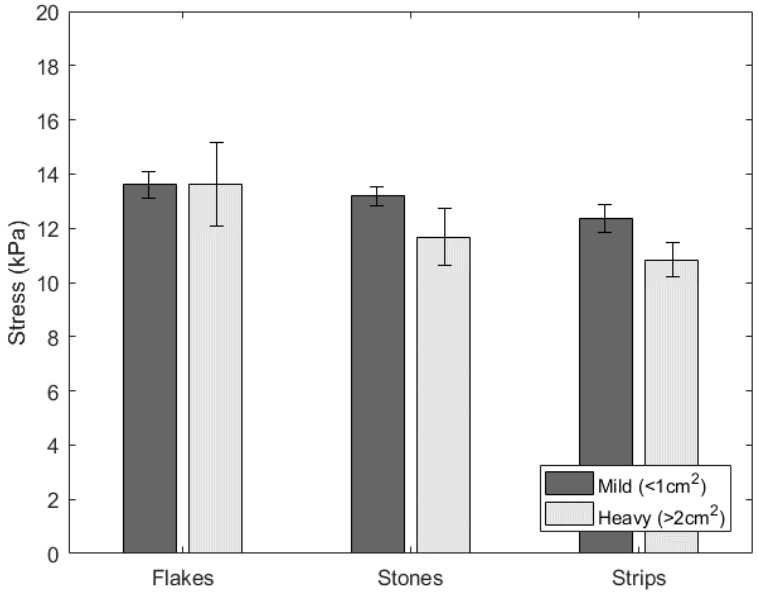

Figure 4.1.2. Comparison of the wall stress of calcified samples based on the calcifications' shape in the PVA sample. The calcifications' surface area was varied from mild (dark grey) to heavy (light grey) (N=3).

A general trend seemed to appear as the degree of calcification is increased, a trend which could reinforce the hypothesis that calcifications have load bearing properties and reduce stress in the nearby wall. The calcifications' shape seems to impact the wall stress, as a decrease is noted from flakes to stones to strips in both mild and heavy calcifications. Stress concentration normally concentrate strongly around sharp irregularities: strip calcifications have sharp ends, much like a spear head, which would increase stress concentration, while stones and flakes usually have more rounded edges. Mock calcifications also have more rounded edges due to the limitations of 3D printing, which may impact the stress concentration effects for normally rough stone and flake calcifications. Large irregularities therefore have an amplified effect on the samples.

4.1.3. Mild vs heavy calcification level – The effect of the area covered in calcifications

A study done by He et al showed that calcifications found in patients' arteries were usually a mix of at least two different shapes, the most common combinations being stones and strips, stones and flakes, as well as stones, strips and flakes together [20]. PVA samples were made to mimic these clinical conditions and determine which had the largest effect on the tissue and in what quantity.

Knowing that average wall stress of baseline PVA is approximately 15 kPa at 15% strain, the decrease in the calcified samples was surprising in Figure 4.1.3. At their highest, the wall stress of these samples was around 10 kPa, a decrease of over 30% in wall stress; at their lowest, a decrease of almost 50%. Even compared to the other mildly and heavily calcified samples tested prior, the decrease in wall stress was quite high.

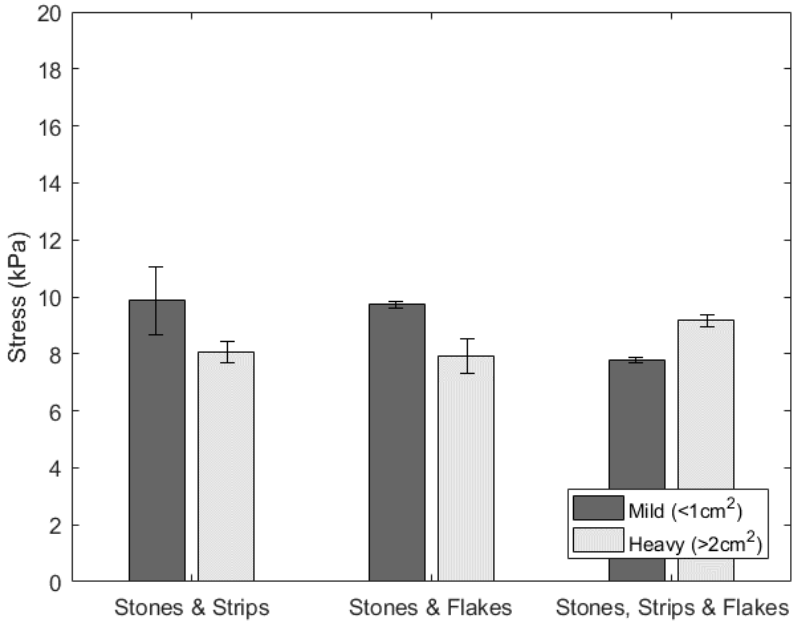

Figure 4.1.3. Comparison of the wall stress of calcified samples mimicking clinical conditions in the PVA sample. The calcifications' surface area was varied from mild (dark grey) to heavy (light grey). N= 3, except the Stones & Flakes – Heavy and Stones, Strips & Flakes - Heavy samples (N=2).

All calcified samples in this group showed no overlap in standard deviation with baseline PVA, having a lower average wall stress than PVA. With the exception of the Stones & Strips samples in mild and heavy calcification, the two other pairs of mock clinical calcifications also showed no overlap in standard deviation between their mild and heavy calcification samples, though it was surprising that the mild samples of Stones, Strips & Flakes had a lower wall stress than their heavy counterpart, especially considering the ongoing trend. In fact, it was the only case of an increase in wall stress in the heavily calcified samples compared to their mildly calcified counterpart. What is clear, however, is that despite the shapes present in the samples, it can be concluded that an increase in calcification load will usually cause a decrease in wall stress.

4.1.4. Adherence

Adherence between the PVA and the calcifications embedded within was evaluated using a uniaxial compression test on approximately 10% of all samples. A displacement of the calcifications within the sample could create pockets that could dissipate the stress. After the compression, the samples were bisected to determine the extent of the adherence. In all samples, total adherence was observed, which contradicted the hypothesis that the reduced wall stress was the result of calcification displacement or the creation of cavities within the sample.

4.2. Finite element analysis

Following the experimental results regarding the load bearing effect of calcifications in PVA samples, finite element models were made to examine how stress accumulated around the calcification and how it impacted the entirety of the sample. Simulated samples mimicked the single calcification samples and underwent similar tensile stretching, but with the mechanical properties of the artery, as these properties had already been used in a number of papers [37, 38]. Simulated samples were subjected to a 15% strain, then analyzed for average wall stress and peak wall stress. Said results from calcified samples were then compared to those of the blank, non-calcified sample.

The average wall stress of all calcified samples showed a strong decrease compared to the non-calcified sample, with the stone calcification showing the smallest decrease in average wall stress while the strip calcification caused the highest decrease. Most of this decreased wall stress could be found around the calcifications, as seen in Figures 4.2.1 to 4.2.3, though calcifications seem to cause stress concentration at the interface between the calcification and the arterial wall. Peak wall stress in all samples was found in the fixed holes, marked in the figures below. Contrary to the trend with the average wall stress, peak wall stress was increased significantly in calcified

samples. The strip calcification sample was the sample with highest decrease in average wall stress, while simultaneously having the highest increase in peak wall stress.

Sample	Average wall stress (kPa)	Diff. (%)	Peak wall stress (kPa)	Diff. (%)
Blank	64.0	-	332.9	-
Flake	45.8	-28.4	440.9	32.5
Stone	49.7	-22.3	417.5	25.4
Strip	36.5	-43.0	469.3	41.0

Table 3. Average wall stress and peak wall stress of finite element model samples. Diff. (%) is the difference in stress between the blank sample and the calcified samples.

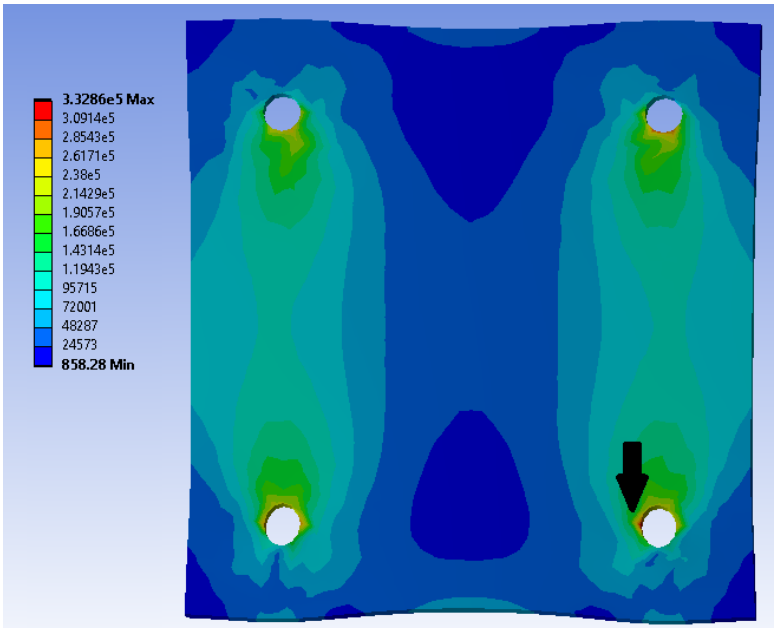

Figure 4.2.1. Cross-section view of the average wall stress of a blank sample. The black arrow highlights peak wall stress. Units in Pascals (Pa).

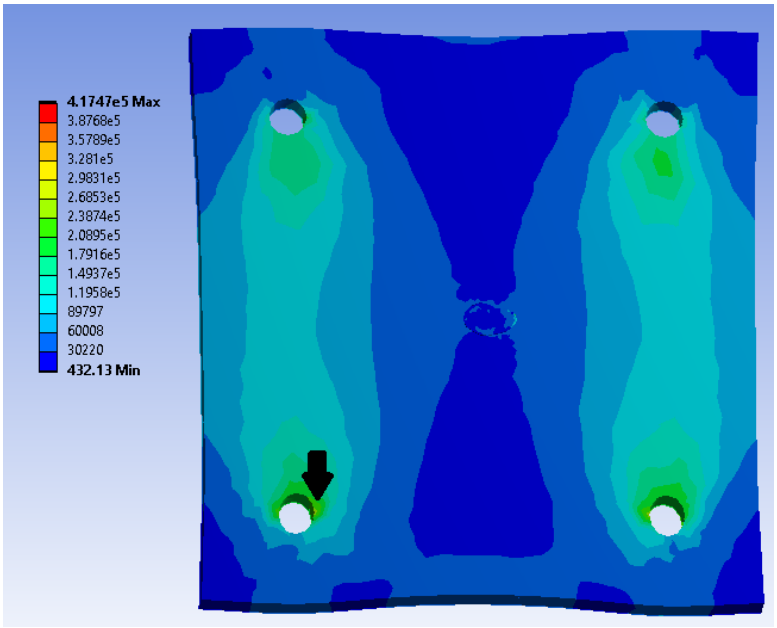

Figure 4.2.2. Cross-section view of the average wall stress of a stone calcification placed in the middle of the sample. The black arrow highlights peak wall stress. Units in Pascals (Pa).

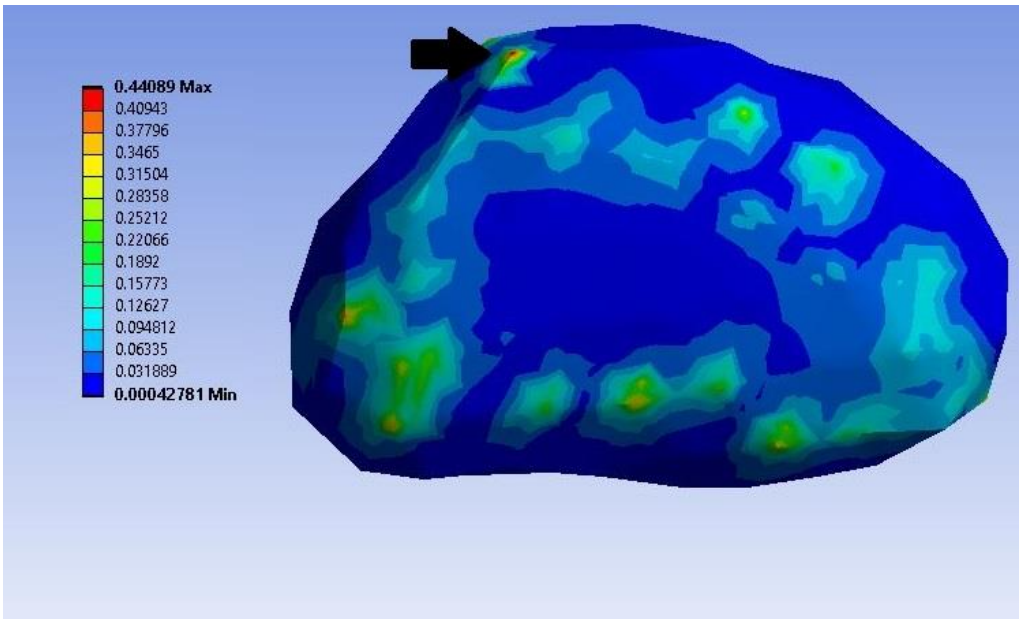

Figure 4.2.3. Stress concentration around flake calcification. Stress accumulated mainly around sharper areas of the calcification, but also decreased quickly the further from edges and irregularities. Black arrow highlights peak wall stress. Units: MPa.

As expected, hook holes created a significant stress concentration effect on the nearby wall, magnifying the stress up to 11 times the average wall stress. Calcifications also had a stress concentration effect on the nearby tissue, though its effect was very limited in range. As seen in Figure 4.2.2, stress accumulated at the interface between the calcification and the arterial wall, but this stress barely expanded beyond the border of the two materials. In Figure 4.2.3, stress is seen to have accumulated at the sharp edges of the calcification, but remained concentrated in such areas, being almost non-existent in flatter surrounding areas.

When compared to the *in vitro* uniaxial tensile testing values, results did not match. In fact, the average wall stress observed in the simulations is three to four times as high as what was observed in their experimental PVA-C counterparts, and their variation was greater than was observed experimentally at that calcification level. In the simulations, a single calcification within the mock arterial wall could cause a decrease of up to 40% of the arterial wall's stress; in comparison, *in vitro* single-calcification PVA had a variation of approximately 15%. Although the mechanical properties reflect those of an artery, they may not be ideal for uniaxial tensile testing in a low-strain regime of 15% strain and under. Of note, the structural effects of calcifications in tissue are not yet clearly understood. Modelling the artery as a linear isotropic elastic material, rather than as a hyperelastic material, in the physiological regime for uniaxial tensile testing showed some interesting results. Defining the material with an elastic modulus of 100 kPa, and a Poisson ratio of 0.2 to mimic the human artery, the results became much more similar to the experimental results.

Type	Average wall stress (kPa)	Diff (%)	Peak wall stress (kPa)	Diff (%)
Blank	13.0	-	74.4	
Flake	14.3	10.0	67.7	-9.0
Stone	13.3	2.3	57.6	-22.6
Strip	15.6	20.0	63.5	-14.7

Table 4. Average wall stress and peak wall stress isotropic elastic finite element model samples. Diff. (%) is the difference in stress between the blank sample and the calcified samples.

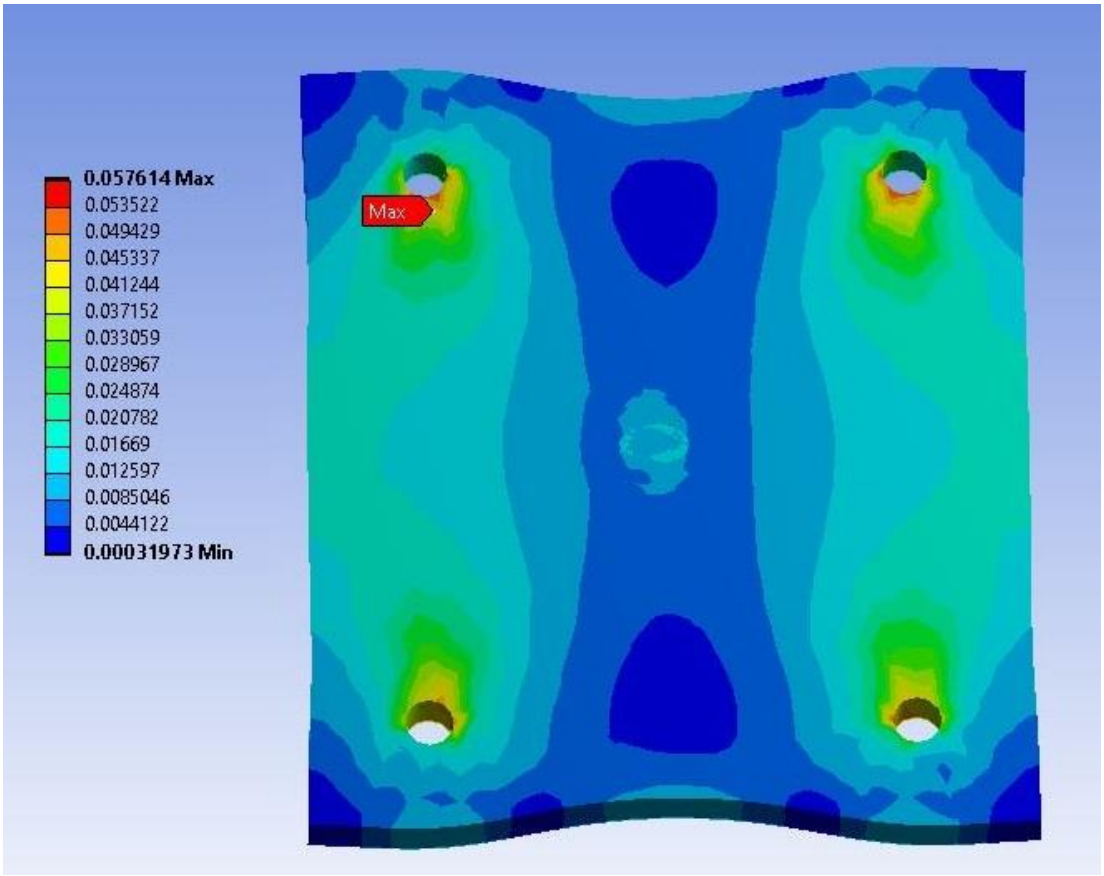

Figure 4.2.4. Cross-section view of the average wall stress of a stone calcification placed in the middle of the sample. Red "Max" pointer highlights peak wall stress. Units in Pascals (Pa).

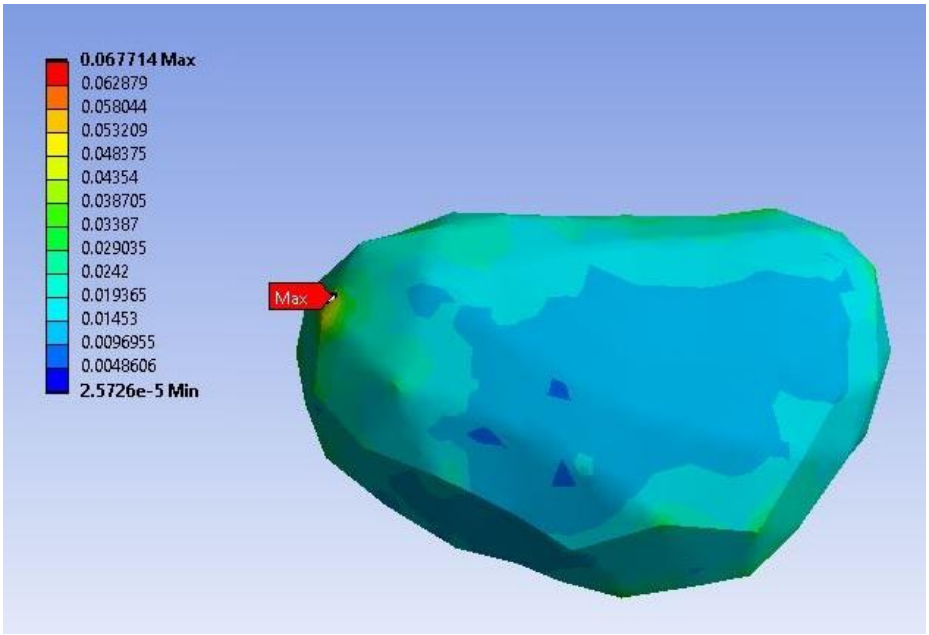

Figure 4.2.5. Stress concentration around flake calcification. Stress accumulated mainly around sharper areas of the calcification, but also dissipated quickly the further from edges and irregularities. Red "Max" pointer highlights peak wall stress. Units: MPa.

The modified simulations demonstrated a much lower average wall stress which correlated more closely with the *in vitro* testing. Average wall stress values for simulated PVA fell within the standard deviation of the experimental PVA, and all simulated samples showed a variation of 20% or less when compared to the simulated PVA which is in line with experimental results. Unlike the previous simulation, average wall stress values of simulated calcified samples were not three to four times their respective experimental values; simulated strip and flake samples were instead within the standard deviation of their experimental counterpart. The simulated stone sample was the only sample which did not fall within the standard deviation of its real-life counterpart, though it may be due to variability in the calcification's position and orientation; its value is however much closer than the previous simulation. Peak wall stress also decreased, as opposed to previous simulations showing an increase.

4.3. Ultrasound imaging of the phantoms

Ultrasound imaging could highlight the lumen of the phantoms. PVA is echogenic enough for ultrasound imaging, though the addition of cellulose in the PVA mix can increase echogenicity. Individual calcifications could not be seen in ultrasound imaging. Following image acquisition as a repetitive pulsatile flow of 20 cm^3 per stroke and an output phase ratio of 35/65 coursed through the phantom, strain was analyzed at over 20 points around the circumference of the lumen at maximum dilatation. Tests were done in duplicate, and all 40 points of the measured strain were plotted in a boxplot. Strain can be defined as the following equation:

$$\varepsilon = \frac{\Delta L}{L_0}$$

where ε represents strain, ΔL represents the change in elongation, and L_0 is the initial length. In this case, the initial length can be assessed as the radius of the lumen (L_0 = 11 mm), while the variation in elongation can be measured as the difference in radius of the lumen as the phantom expands during the pulsatile flow. Global and local strain were analyzed from the same acquired images: the former representing the strain analysis along the entire circumference of the lumen, and the latter being only an analysis of the calcified portion of the phantom.

4.3.1. Global mean strain

The median strain for the baseline PVA was found around 8% strain, with most values being between 7% and 10% (Figure 4.3.1). Calcified phantoms showed strong overlaps among themselves and with the blank phantoms, though their medians differed. Only two outliers were seen: one in the blank, or baseline, PVA phantoms and one in the Stones & Flakes phantoms; both identified in the boxplot (Figure 4.3.1) as red crosses. These outliers were potentially caused by a small fissure or air pocket in the mock arterial wall which led to a high strain. These values were

excluded from further analysis due to their extreme differences from the rest of their respective samples.

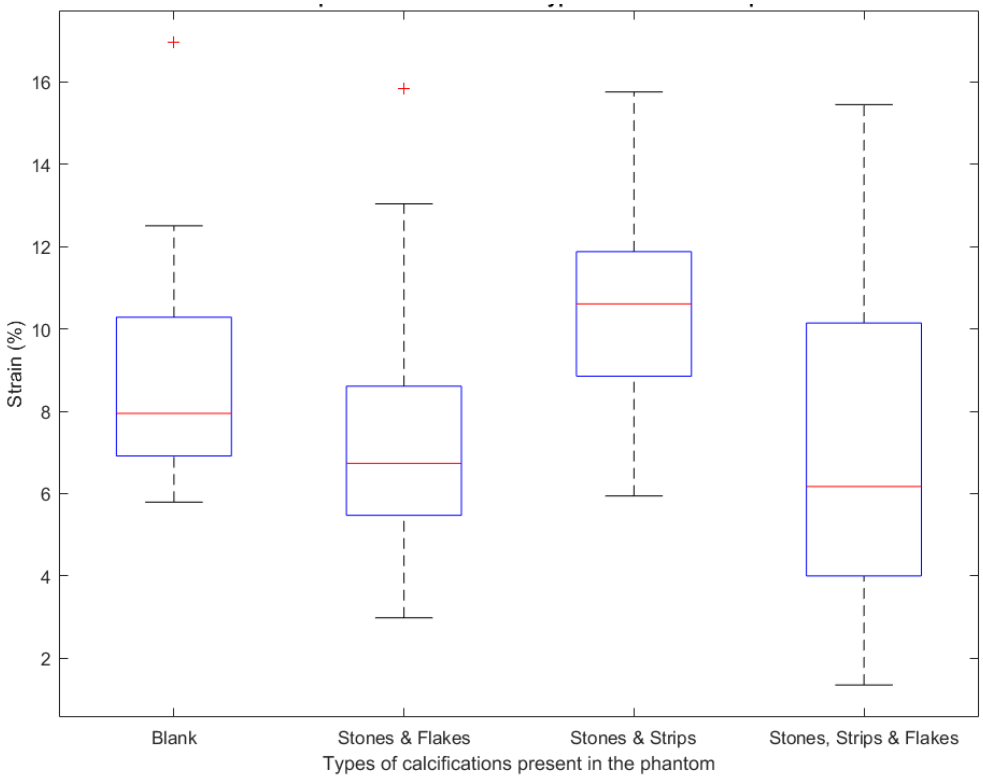

Figure 4.3.1. Boxplot of global strain in mock arterial phantoms based on the types of calcifications present within the arterial wall. Red line is the median of the duplicate tests for a specific phantom; blue box represents the second and third quarters of the data; the lower and upper whiskers represent the first and fourth quarters respectively; and the red crosses are outliers.

The Stone & Flakes phantoms and the Stones, Strips & Flakes phantoms showed a small decrease in strain compared to the blank phantoms, which could be translated as an increase in elastic modulus, while the Stones & Strips phantoms showed a greater increase in strain and therefore a decrease in elastic modulus.

Phantom composition	Global mean strain (%)	n	Diff (%)
PVA	8.72 ± 2.36	2	-
Stones & Flakes	7.35 ± 2.64	2	-15.71
Stones & Strips	10.46 ± 2.28	2	19.95
Stones, Strips & Flakes	7.17 ± 3.75	2	-17.78

Table 5. Global mean strain of phantoms when analyzed with ultrasound imaging.

These variations were also reflected in Table 5 where their individual means are compared to that of the blank phantoms. Their strong overlap with the blank phantom in the boxplot format was already an indicator of their similarity, and comparison of their standard deviation confirmed the lack of a significant difference between phantoms. In this situation, this significant overlap in strain may have been due to a more global analysis rather than a local analysis of PVA surrounding the calcifications.

4.3.2. Local mean strain

Local mean strain was analyzed in the calcified portion of the phantoms. Unsurprisingly, as seen in Figure 4.3.2 and Table 6 below, local median strain for the blank phantom, which was analyzed in a non-calcified portion of the phantom adjacent to the calcified area, remained very similar to its global counterpart, being once again centered around an 8% strain, and varying between 7% and 10%.

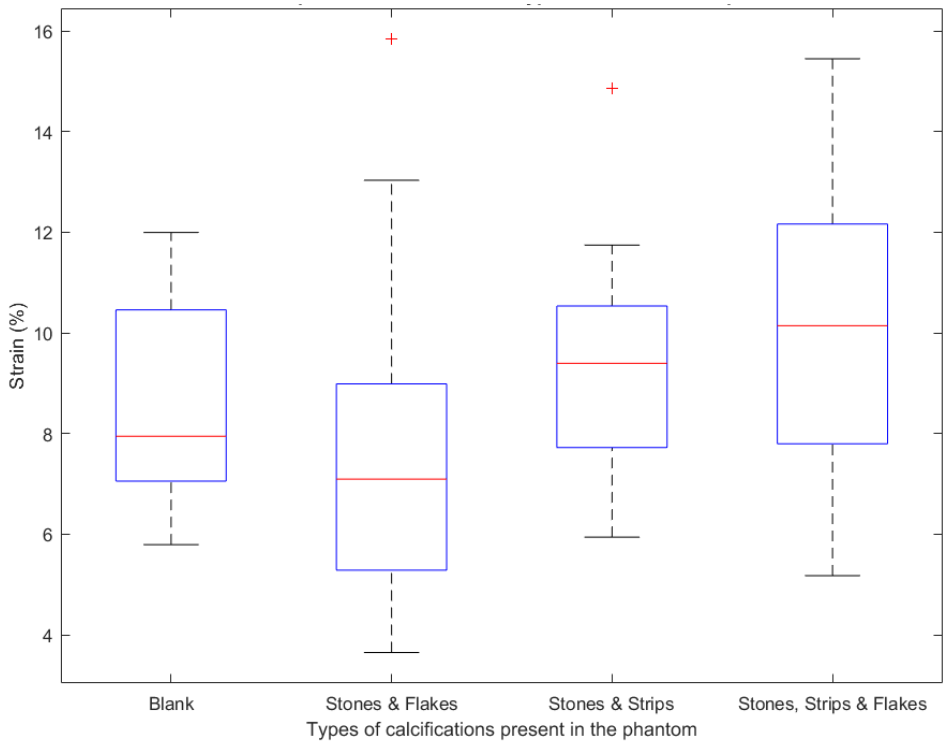

Figure 4.3.2. Boxplot of local strain in mock arterial phantoms based on the types of calcifications present within the arterial wall. Red line is the median of the duplicate tests for a specific phantom; blue box represents the second and third quarters of the data; the lower and upper whiskers represent the first and fourth quarters respectively; and the red crosses are outliers.

Phantom composition	Local mean strain (%)	n	Diff (%)
PVA	8.63 ± 1.95	2	-
Flakes and stones	7.80 ± 3.31	2	-9.62
Strips and stones	9.35 ± 2.02	2	8.34
Flakes, strips and stones	10.04 ± 2.92	2	16.34

Table 6. Local mean strain of phantoms when analyzed with ultrasound imaging.

Meanwhile, the Stones & Strips phantoms showed a slight decrease in median strain and a significant increase in boxplot overlap with the blank phantom; inversely, the Stones, Strips &

Flakes phantoms showed instead a significant increase in median strain. Much like the previous test, two outliers were seen: one in the Stones & Flakes phantoms and one in the Stones & Strips phantoms (Figure 4.3.2) and were identified as red crosses. These values were once again excluded from further analysis. In Table 6 above, analysis of the local mean strain showed once again a strong resemblance between baseline PVA phantoms and calcified phantoms. The local analysis of the calcified phantoms showed less variation than their previous global evaluation.

5. Discussion

Results from uniaxial tensile testing, finite element analysis and ultrasound imaging of phantoms showed an interesting portrait, pointing to a general load bearing effect due to the presence of calcifications in the PVA matrix. Uniaxial tensile testing demonstrated that increasing the calcification volume within small PVA samples led to a strong decrease in wall stress, one that became clear as calcification volume increased. At 15% strain, the wall stress of baseline PVA samples was almost twice as high as the most calcified clinical samples, which seems to support the theory that calcifications have a load bearing effect on the arterial wall and may reduce the stress in the nearby wall: they reduced the overall stress in the wall as their number increased. An initial hypothesis supposed that an increase in calcifications within a fixed sample size would reduce the amount of PVA holding the entire sample together, which would lead to a weaker overall structure. The presence of additional calcifications in the mock tissue could cause issues with adherence and create pockets that could dissipate stress. Adherence testing of calcified samples showed a strong adherence between calcifications and PVA, which may be due to the similar chemical nature of these PVA-based mock tissues. As these mock tissues underwent freezing and thawing cycles together, it is possible that PVA molecules bonded between the PVA-based calcifications and the mock arterial wall, causing the strong adherence that was observed. The evaluation of the shapes of calcifications seemed to point to flake calcification having less of an effect on nearby tissue than stone and strips calcifications, probably due to strips having sharp edges and inducing more stress concentration near their tips.

Meanwhile, finite element analysis of a single calcification in a human tissue analog demonstrated that calcium deposits in the tissue did two things: they significantly reduced the peak wall stress of the sample, and the calcifications caused small stress concentration in surrounding

tissues over a much more limited range than previously thought. In fact, considering the much higher elastic modulus of calcifications when compared to the arterial tissue, it was believed calcifications would greatly affect the general surrounding area. However, finite element analysis of all three shapes of calcifications highlighted the short area of stress concentration effect calcifications have on the tissue. Although all three shapes created a form of stress concentration around them, this effect was extremely localized, and surrounding tissues had instead a strong reduction in peak wall stress when compared to non-calcified samples. As expected, this stress concentration was mainly concentrated around sharper edges, such as the tips and ends of the calcifications, but it was also found along the entire calcifications to a different degree (Figure 4.2.3). Single calcification samples that underwent uniaxial tensile testing showed some variation in wall stress when compared to the blank sample, a similar response to the results of the finite element analysis. Numerical models where the sample was assumed to be a linear isotropic elastic material instead of hyperelastic showed a 10% to 20% variation in wall stress which was within the range of variation in physical models. On that note, it is possible that a Mooney-Rivlin hyperleastic model may have been a better fit to simulate tissue in low strain regime, rather than a Yeoh hyperelastic model. Regarding the comparison between numerical and experimental models, both *in vitro* and numerical samples showed a 10 to 20% variation due to many factors: a single calcification could not always be placed at the same position, the same angle and the same depth. Even so, were it the case, the expansion and contraction of PVA during its freezing and thawing cycles can always lead to unexpected movements of the calcification within the samples. Hole piercing, hooking and installing the sample on the uniaxial tensile testing machine may also have led to changes in the overall structure of the sample, something that is difficult to represent correctly in a finite element model. However, samples exhibiting higher levels of calcifications

did highlight the load bearing effect of calcifications, as the wall stress of the samples diminished significantly. An important factor to consider in uniaxial tensile testing was the calcification's shape. Physical calcifications and their finite element models have sharp microscopic edges that increase stress concentration and affect the surrounding area; PVA-based calcifications made out of a mould could not retain the microscopic edges due to the limitations of 3D printing and were therefore much rounder in shape, which may explain the lack of significant results in single calcification samples. Only their ends and curves could create stronger stress concentrations around the calcifications.

In uniaxial tensile testing samples, heavily calcified samples had an approximate 9:1 volume ratio of calcifications to baseline PVA holding the samples together. In AAA phantoms, this volume ratio is massively decreased due to the large size of the phantom, which led to heavy calcifications only representing approximately 1% of the total volume of the phantoms. Strain analysis in ultrasound images demonstrated a strong overlap in strain values in blank and calcified phantoms, which is mainly due to the calcifications having a very localized effect on surrounding tissues and said surrounding tissue being able to dissipate the stress over a much larger area than the uniaxial tensile samples. As demonstrated in the elastic modulus formula:

$$E = \frac{\sigma}{\epsilon}$$

where E represents the elastic modulus, σ the pressure, and ε the strain, an increase in strain at a constant pressure causes a decrease in elastic modulus. This increase in overall strain can be observed in the local analysis of Stones & Strips and Stones, Strips & Flakes phantoms, while Stones & Flakes phantoms showed a decrease in overall strain: the two former phantoms showed a decrease in elastic modulus similar to the uniaxial tensile testing samples. It is possible that the

phantoms did not show a more significant decrease due to calcification displacement during the freezing and thawing process: what was once a very dense mix of calcification and PVA in localized areas of the phantom may have become a mildly calcified area instead, which would alter results. Unlike uniaxial tensile testing samples, calcifications could not be confined to a small restricted area.

Although the results varied from one type of test to another, these variations highlighted the effects of calcifications in tissues. As stated previously, when placed under stress, calcifications had a stress concentration effect on surrounding tissues, though this effect was extremely localized. This effect extended about a millimeter from the edge of the calcification before the stress dissipated into the tissue. Stress concentration around calcifications were at their strongest near sharp edges or irregularities, as is usually the case in such situations. Moreover, this effect was observed around every calcification, but seemed to be amplified as the density of calcifications increased within the PVA sample. This amplification was only noticeable in densely calcified areas in the uniaxial tensile testing samples, while it was observable in finite element models with a single calcification. Samples with low calcium deposit density, such as the single calcification testing samples, exhibited little to no difference in wall stress compared to baseline PVA samples, as seen in the statistical analysis. Despite some stress accumulating around the calcifications, the load bearing effect of calcifications seemed to be much more effective, causing stress in nearby tissue to be reduced, which would explain the decrease in wall stress of PVA samples. In addition, it seemed clinical cases of calcifications, which were the uniaxial samples and phantoms with mixed calcification shapes (Stones & Flakes, Stones & Strips, and Stones, Strips & Flakes), had a much stronger load bearing effect than non-clinical cases, which suggested that calcification shape may have a larger effect on the surrounding tissue.

The analysis of volume ratios of PVA and calcium deposits demonstrated the limits of the ratio between PVA and the calcifications placed within the samples (Tables 7 & 8). Knowing that each element of the PVA samples and phantoms had a precise volume, ratios could be established to determine the relative presence of calcifications. Increase in calcification in PVA samples was previously mentioned to be the main factor behind the variation in wall stress. Single-calcification samples, in which the calcification represents up to approximately 10% of the uniaxial tensile testing sample, demonstrated little variation in wall stress. Even in the flake sample, where the ratio was around 10%, the stress concentration and load bearing effects of calcifications were too limited to effectively affect the PVA. In AAA phantoms, calcifications represented a very small portion of the entire volume and may have been more dispersed during the curing, leading to low variation in global strain compared to baseline PVA.

Sample	Volume (mm^3)
Uniaxial tensile testing sample	562.5
Stone calcification	3.2
Strip calcification	16.2
Flake calcification	59.6
Phantom (without aneurysm)	13695.4
Phantom (with aneurysm)	37257.3
Mild calcification (1 cm^2)	250
Heavy calcification (2 cm^2)	500

Table 7. Volume of each element used to make the samples and phantoms.

However, in the more calcified uniaxial tensile testing samples, where calcifications represented 40% to 90% of the entire volume, a stark change could be seen. The variations in wall stress became much more significant when the volumetric ratio was increased to 40% and more, though this variation was much more pronounced in clinical samples. Thus, a significant increase in calcification volumetric ratio led to a stronger variation in wall stress of PVA samples.

Sample type	Ratio (%)
Single stone calcification in uniaxial tensile testing sample	0.6
Single strip calcification in uniaxial tensile testing sample	2.9
Single flake calcification in uniaxial tensile testing sample	10.6
Mild calcification (1 cm^2) in uniaxial tensile testing sample	44.4
Heavy calcification (2 cm^2) in uniaxial tensile testing sample	88.9
AAA phantom with mild calcification (1 cm^2)	0.7
AAA phantom with heavy calcification (2 cm^2)	1.3

Table 8. Volumetric ratio of each tested sample.

5.1. Limitations

A major difficulty in this study was the limited laboratory access due to the COVID-19 pandemic. This difficulty limited the number of samples and phantoms that could be made, both for the uniaxial tensile testing and the ultrasound imaging, and was an additional factor as to why the samples in these experiments had to undergo manual freezing and thawing cycles instead of automatic thermal cycles. Although the difference between the two methods of cycling PVA is minimal when done correctly, automatic cycling would have been preferred to obtain more consistent results. Manual thermal cycling can cause slight variations in the mechanical properties

of PVA-C due to the lack of control over freezing and thawing rates: this constraint had to be managed by testing every sample in duplicate or triplicate to reduce variation. More so, the baseline PVA-C's mechanical properties were validated with PVA that had been subjected to automatic thermal cycling. The samples were also placed on a damp plate and sealed in a previously soaked plastic bag in order to prevent the samples from drying off during the freezing and thawing process. Previous tests of non-sealed, manually cycled samples demonstrated significant dryness of samples which affected their mechanical properties. Swelling of PVA during the freezing and thawing process also led to some variation in calcification orientation and depth. Calcifications were placed in the PVA hydrogel before its curing, their depth and orientation within the sample determined at this moment. However, due to the uncontrollable nature of the expansion and contraction of PVA during its thawing and freezing phases, respectively, calcifications which once had a specific orientation and depth were pushed around. This led to many samples having calcifications either too close to the surface or even piercing through it, or samples with either high or low calcification density due to drifting during the curing. This issue was the main reason that the uniaxial tensile testing samples used to examine the effects of calcification's depth only included a single calcification: it was much easier to control and readjust the position of a single calcification than that of twenty.

Regarding PVA making, air bubbles were a major issue in moulds. When pouring PVA in a mould, small pockets of air would form and remain there during the freezing and thawing process, leading to weaknesses in the PVA which caused stress concentration and negatively affected results. To remedy to this issue, moulds had to be opened after their first thawing to verify the integrity of the PVA, then air bubbles were pierced if any were found and additional PVA was added in the crevasse. Usually, most air bubbles were dealt with in this situation and the PVA was

able to retain a strong homogeneity. In cases where air bubbles were found past the second thawing, the samples were discarded completely.

Ultrasound imaging of the PVA phantoms was done with a pure PVA mix, but an article published by Fromageau suggested the use of cellulose in order to increase the echogenicity of the phantoms or the calcifications [40]. An increase in the echogenic nature of calcifications would have made them easier to see in ultrasound images and increased the quality of the strain analysis done on the phantom.

6. Conclusion

6.1. Significance

This study demonstrated the feasibility of creating mock calcifications with similar mechanical properties to that of real calcifications and introducing them in PVA phantoms. The insertion of calcifications in PVA models demonstrated their strong load bearing effect on surrounding tissue, and their limited stress concentration effect. Uniaxial tensile testing confirmed the decrease of stress in calcified samples when compared to non-calcified samples, while finite element models illustrated the load bearing aspect of calcifications and the limited area of stress concentration surrounding the calcifications. Finally, PVA phantoms showed an increase in strain in calcified areas, which marked a decrease in elastic modulus similar to the one seen in all previous tests. Results indicated a strong relation between high calcification presence and stress reduction, and it would be interesting to push this research even further by testing the effect of calcification on catheter insertion and deployment. Increasing calcification presence to match that of damaged AAA would certainly clarify some of the shortcomings of SG deployment.

6.2. Future works

Further research on calcifications in PVA should focus first on potentially replicating the tests of the calcified phantoms with a larger number of samples, since limited resources and laboratory access made it difficult to do more testing in this study. Testing these additional calcified phantoms under mock clinical conditions would give more insight into the effect of calcifications in phantoms. Additional research could characterize the biaxial properties of mild and heavily calcified samples as well as analyze the effect of helicoidal topology of calcification in mock AAA phantoms. Calcium deposits can often be found following a helicoidal topology in calcified aortas, a structural phenomenon which would be interesting to examine in order to determine this effect on the arterial wall stress. Furthermore, rather than investigating calcifications by their shape when increasing calcification presence, further research should instead focus on creating larger calcification plaques, which are often found in more calcified arteries, as they are more stable and have a fixed size, thus reducing the calcification displacement bias while mimicking clinical conditions.

7. References

7.1. List of references

1. McKinley, M., O'Loughlin, V., Pennefather-O'Brien, E. (2016). *Human Anatomy (5th Edition)*. Boston: McGraw-Hill Higher Education.
2. Berillis, P. (2013). *The role of collagen in the aorta's structure*. The Open Circulation and Vascular Journal, 6, 1-8. 1877-3826/13.
3. Johnson, R.C., Leopold, J.A., Loscalzo, J. (2006). *Vascular calcification: pathobiological mechanisms and clinical implications*. Circulation Research, 1044-1059. DOI: 10.1161/01.RES.0000249379.55535.21.
4. Ebrahimi, A.P. (2009). *Mechanical properties of normal and diseased cerebrovascular system*. Journal of Vascular and Interventional Neurology, 2(2), 155-162
5. Alberts, B., Johnson, A., Lewis, J., Raff, M., Roberts, JK., Walter. P. (2002*). Molecular Biology of the Cell. 4th Edition*. Garland Science. New York.
6. Siegel, C.L., Cohan, R.H., Korobkin, M., Alpern, M.B., Courneya, D.L., Leder, R.A. (1994). *Abdominal aortic aneurysm morphology: CT features in patients with ruptured and nonruptured aneurysms*. American Roentgen Society. 0361-803X/94/1635-1123.
7. Barrett, H.E, Cunnane, E., Hidayat, H., O'Brien, J., Moloney, M.A., Kavanagh, E.G., Walsh, M.T. (2017). *On the influence of wall calcification and intraluminal thrombus on prediction of abdominal aortic aneurysm rupture*. Society of Vascular Surgery. http://dx.doi.org/10.1016/j.jvs.2017.05.086.
8. Koole, D., Zandvoort, H., Schoneveld, A., Vink, A., Vos, J., van den Hoogen, L., de Vries, J.P., Pasterkamp, G., Moll, F., van Herwaarden, J. (2013). *Intraluminal abdominal aortic aneurysm thrombus is associated with disruption of wall integrity*. Society for Vascular Surgery. http://dx.doi.org/10.1016/j.jvs.2012.07.003.
9. Hermann, M, Lehmann, N., Gronewold, J., Baeur, M., Mahabadi, A., Weimar, C., Berger, K., Moebus, S., Jockel, K.H., Erbel, R., Kalsch, H. (2015). *Thoracic aortic calcification is associated with incident stroke in the general population in addition to established risk factors*. European Heart Journal – Cardiovascular Imaging, 16, 684-690. doi:10.1093/ehjci/jeu293.

10. Fillinger, M.F., Raghavan, M.L., Marra, S.P., Cronenwett, J., Kennedy, F. (2002*). In vivo analysis of mechanical wall stress and abdominal aortic aneurysm rupture risk*. Society for Vascular Surgery. doi:10.1067/mva.2002.125478.
11. Hans, S.S., Jareunpoon, O., Balasubramaniam, M., Zelenock, G.B. (2005). *Size and location of thrombus in intact and ruptured abdominal aortic aneurysms*. Society for Vascular Surgery. doi:10.1016/j.jvs.2005.01.004.
12. Zhu, C., Leach, J., Wang, Y., Gasper, W., Saloner, D., Hope, M. (2020). *Intraluminal thrombus predicts rapid growth of abdominal aortic aneurysms*. Radiology, 294, 707–713. https://doi.org/10.1148/radiol.2020191723.
13. Fillinger, M.F., Racusin, J., Baker, R., Cronenwett, J., Teutelink, A., Schermerhorn, M., Zwolak, R., Powell, R., Walsh, D., Rzucidlo, E. (2004). *Anatomic characteristics of ruptured abdominal aortic aneurysm on conventional CT scans: implications for future risk*. Society for Vascular Surgery. doi:10.1016/j.jvs.2004.02.025.
14. Joshi, F.R., Rajani, N., Abt, M., Woodward, M., Bucerius, J., Mani, V., Tawakol, A., Kallend, D., Fayad, Z., Rudd, J. (2016*). Does vascular calcification accelerate inflammation? A substudy of the dal-PLAQUE trial*. Journal of the American College of Cardiology, 67, 69-78. http://dx.doi.org/10.1016/j.jacc.2015.10.050.
15. Chowdhury, M.M., Zielinkski, L., Sun, J., Lambracos, S., Boyle, J., Harrison, S., Rudd, J., Coughlin, P. (2018). *Calcification of thoracic and abdominal aneurysms is associated with mortality and morbidity*. European Journal of Vascular and Endovascular Surgery, 55, 101-108. https://doi.org/10.1016/j.ejvs.2017.11.007
16. Toussaint, N.D., Kerr, P. (2007). *Vascular calcification and arterial stiffness in chronic kidney disease: implications and management*. Nephrology, 12, 500-509. doi:10.1111/j.1440-1797.2007.00823.x.
17. Cahalane, R.M., Barrett, H.E., O'Brien, J.M, Kavanagh, E.G., Moloney, M.A., Walsh, M.T. (2018). *Relating the mechanical properties of atherosclerotic calcification to radiographic density: A nanoindentation approach*. Acta Biomaterialia, 80, 228-236. https://doi.org/10.1016/j.actbio.2018.09.010
18. Meeker, D.R., Kesten, H.D. (1936). *Composition of pathological calcium deposits*. J. Biol. Chem., 113, 289-296.

19. Sakalihasan, N., Michel, J.B. (2009). *Functional imaging of atherosclerosis to advance vascular biology*. European Journal of Vascular and Endovascular Surgery, 37(6), 728-734. doi:10.1016/j.ejvs.2008.12.024
20. He, Z., Mongrain R., Lessard S., Soulez G. (2018). *Extents, locations and geometrical configurations of calcification in abdominal aortic aneurysm*. In: Eskola H., Väisänen O., Viik J., Hyttinen J. (eds) EMBEC & NBC 2017. EMBEC 2017, NBC 2017. IFMBE Proceedings, vol 65. Springer, Singapore. https://doi.org/10.1007/978-981-10-5122-7_160
21. Yang C-J, Tsai S-H, Wang J-C, Chang WC, Lin C-Y, Tang Z-C, Hsu H-H. (2019). *Association between acute aortic dissection and the distribution of aortic calcification*. PLoS ONE 14(7): e0219461. https://doi.org/10.1371/journal.pone.0219461
22. Maier, A., Gee, M.W., Reeps, C., Eckstein, H.H., Wall, W.A. (2010). *Impact of calcifications on patient-specific wall stress analysis of abdominal aortic aneurysms*. Biomechanics and Modeling in Mechanobiology, 9, 511–521. DOI 10.1007/s10237-010-0191-0.
23. He, Z., Mongrain, R., Lessard, S., Chayer, B., Cloutier. G., Soulez, G. (2020). *Anthropomorphic and biomechanical mockup for abdominal aortic aneurysm*. Medical Engineering & Physics, vol. 77, 60-68. https://doi.org/10.1016/j.medengphy.2019.12.005
24. Pazos, V., Mongrain, R., Tardif, J.C. (2010). *Deformable mock stenotic artery with a lipid pool*. Journal of Biomechanical Engineering 2010;132:034501. doi:10.1115/1.4000937.
25. Pazos, V., Mongrain, R., Tardif, J.C. (2010). *Mechanical characterization of atherosclerotic arteries using finite-element modeling: feasibility study on mock arteries*. IEEE Transactions on Biomedical Engineering 2010;57:1520–8. doi:10.1109/TBME.2010.2041001.
26. Youssef, S. (2012). *Experimental analysis of a mock atherosclerotic calcified coronary artery*. [Dissertation]. Montréal (QC): McGill University.
27. Greenhalgh RM, Brown LC, Powell JT, Thompson SG, Epstein D, Sculpher MJ (2010). *Endovascular versus open repair of abdominal aortic aneurysm*. New England Journal of Medicine, 362(20), 1863-1871. doi:10.1056/NEJMoa0909305
28. Acosta, S., Lindblad, B., Zdanowski, Z. (2007). *Predictors for outcome after open and endovascular repair of ruptured abdominal aortic aneurysms*. European Journal of Vascular and Endovascular Surgery, 33(3), 277-284. doi:10.1016/j.ejvs.2006.09.017
29. Roy, D. (2015). *Mechanical simulation of the endovascular repair of abdominal aortic aneurysms*. [Dissertation]. Montréal (QC): Université de Montréal.

30. Schermerhorn, M.L., Buck, D.B., O'Malley, A.J., Curran, T., McCallum, J., Darling, J., Landon, B. (2015). *Long-term outcomes of abdominal aortic aneurysm in the Medicare population*. New England Journal of Medicine, 373(4), 328-338. doi:10.1056/NEJMoa1405778
31. Jaramillo, T. (2019). *Human heart phantom for catheter navigation assessment*. [Dissertation]. Montréal (QC): McGill University.
32. Nazanin, A. (2016*). Mechanical properties of poly (vinyl alcohol) based blends and composites*. [Dissertation]. University of Western Ontario. Electronic Thesis and Dissertation Repository. 3746. https://ir.lib.uwo.ca/etd/3746
33. Pazos, V., Mongrain, R., Tardif, J.C. (2009). *Polyvinyl alcohol cryogel: optimizing the parameters of cryogenic treatment using hyperelastic models*. Journal of the Mechanical Behaviour of Biomedical Materials 2009;2:542–9. doi:10.1016/j.jmbbm.2009.01.003.
34. Wan, W.K., Campbell, G., Zhang, Z.F., Hui, A.J., Boughner, D.R. (2002). *Optimizing the tensile properties of polyvinyl alcohol hydrogel for the construction of a bioprosthetic heart valve stent*. Journal of Biomedical Material Resistance (Appl Biomater), 63, 854–861.
35. Wan, W., Bannerman, A.D., Yang, L. Mak, H. (2014*). Poly(Vinyl Alcohol) Cryogels for biomedical applications*. Polymeric Cryogels, Advances in Polymer Science 263. DOI 10.1007/978-3-319-05846-7_8.
36. Zikry, C., Mongrain. R., Cartier, R., Soulez, G. (2018). *Evaluation of poly(vinyl alcohol) cryogel as viscoelastic reconstruction graft for the ascending aorta*. [Dissertation]. Montréal (QC): McGill University.
37. Mohammadi, H., Cartier, R., Mongrain, R. (2018). *Fiber-reinforced computational model of the aortic root incorporating thoracic aorta and coronary structures*. Biomechanics and Modeling in Mechanobiology, 17, 263–283. https://doi.org/10.1007/s10237-017-0959-6.
38. Strube, H., Mongrain, R. (2019). *Treatment of abdominal aortic aneurysms: influence of wall calcifications*. [Report]. Montréal (QC): McGill University.
39. Yushkevich, P.A., Piven, J., Hazlett, H.C., Smith, R.G., Ho, S., Gee, J.C., Gerig, G. (2007). *User-guided 3D active contour segmentation of anatomical structures: Significantly improved efficiency and reliability*. Neuroimage 2006 Jul 1;31(3):1116-28.
40. Fromageau, J., Gennisson, J.L., Schmitt, C., Maurice, R., Mongrain, R., Cloutier, G. (2007). *Estimation of polyvinyl alcohol cryogel mechanical properties with four ultrasound*

elastography methods and comparison with gold standard testings. IEEE Transactions on ultrasonics, ferroelectrics and frequency control, vol. 54, No. 3, 498-509.

41. Farber, M., Parodi, F.E. (2020). Abdominal aortic branch occlusion. Merck Manual, Merck & Co. URL Adress of image: https://www.merckmanuals.com/en-ca/home/heart-and-blood-vessel-disorders/aneurysms-and-aortic-dissection/abdominal-aortic-branch-occlusion.
42. Case courtesy of Dr Hani Makky Al Salam, Radiopaedia.org, rID: 8190.
43. Case courtesy of Dr Jeremy Jones, Radiopaedia.org, rID: 10122.
44. Case courtesy of Associate Professor Donna D'Souza, Radiopaedia.org, rID: 3828.
45. Endovascular Aneurysm Repair (2020). UCSF Department of Surgery.